**OAK RIDGE
NATIONAL LABORATORY**

MANAGED BY UT-BATTELLE
FOR THE DEPARTMENT OF ENERGY

NUCLEAR CROSS-SECTION CALCULATIONS IN THE 1 MEV TO 5 GEV RANGE WITH COMBINED SEMI-CLASSICAL AND QUANTUM MECHANICAL MODELS

February 2002

Prepared by
F. B. GUIMARÃES , C. Y. FU AND L. C. LEAL

UT-BATTELLE

ORNL-27 (4-00)

Nuclear Science and Technology

NUCLEAR CROSS-SECTION CALCULATIONS IN THE 1 MEV TO 5 GEV RANGE WITH COMBINED SEMI-CLASSICAL AND QUANTUM MECHANICAL MODELS

F. B. GUIMARÃES , C. Y. FU AND L. C. LEAL

February 2002

Contents

<h1 style="text-align:center">List of Figures</h1>

ABSTRACT

In this work we describe neutron and proton induced reaction cross-sections for iron produced by the codes TNG and CEM95 in the 5 to 300 MeV energy range. TNG calculations cover the 5-90 MeV range, while CEM95 covers the 50-300 MeV high energy range. The two codes show some disagreements in the overlap energy range, both among themselves and with the experimental data, which are presently being addressed. The experimental data used are from NNDC and/or from LA150 NSE references. We also describe some developments for combining TNG and CEM95 into a new code called CETNG (Cascade Exciton TNG).

I. INTRODUCTION

There is an increasing need to extend the upper limit of energy of the Evaluated Nuclear Data File (ENDF/B-VI) to high energies, e. g., to 150 MeV and above, for various technological and scientific applications [1]. Technologies such as the Spallation Neutron Source (SNS) or the accelerator production of tritium or the transmutation of long-lived radioactive nuclides into shorter- lived ones for the treatment of nuclear waste need high energy nuclear data up to a few GeV. As yet, no model code covers this wide range of energies.

In the present work we address this problem by developing a consistent nuclear cross-section code usable from the high-keV to low-GeV range, in which the semi-classical to quantum transition is accurately done. This goal can be achieved with two codes already in use at the Oak Ridge National Laboratory (ORNL), CEM95 [2] and TNG [3], complemented by the development of new models which implement a continuous transition between quantum and semi-classical regions.

CEM95 is a semi-classical high-energy nuclear cross-section model code for incident energies from about 20 MeV to a few GeV developed by Stepan G. Mashnik *et al.* [2]. It has been incorporated into the ORNL high-energy transport code, HETC [4], as an alternative to the HETC original cross-section model that combines the intranuclear cascade model (INC) of Bertini [5] with an evaporation model (EVAP) in accordance with the original formulation of Bethe [6]. CEM95 is a good alternative among the semi-classical model codes because it correctly uses the pre-equilibrium (PE) model to link the INC and EVAP models. On the other hand, the code TNG is a nuclear cross-section model code for lower energies, from the keV region to about 90 MeV, developed at the ORNL and continuously updated as a tool for cross section evaluation.

Due to the capabilities of CEM95 and TNG, the incident energy range of the new code, hereafter called CETNG, ranges from about 1 MeV to 5 GeV. CETNG will allow data evaluation for a large number of materials whose cross-section data are needed for a wide range of applications, including the SNS design and accelerator driven systems.

In the following sections we briefly describe the available models that have been used in this work and some developments for the new code. Results of calculations using TNG, CEM95 and CETNG are compared with experimental results.

II. DESCRIPTION OF THE REACTION PROCESS

To achieve a consistent description of nuclear reactions one uses different models for the various energy regions.

In the highest energy region (above 150 MeV) the reaction process can be described by the semi-classical INC model. In this case one assumes that the components of the initial and final channels can be treated semi-classically as "particles" instead of "waves" in the description of their motion between two successive collisions.

For energies below a given threshold in a reaction process two PE models are needed. One PE model suitable for energies in the range 20–40 MeV, in which the semi-classical description is still valid, and

another one for energies below this region, in which the PE decay is described quantum-mechanically and spins and parities are conserved. Finally, it is necessary to use a model based on the formalism of Hauser-Feshbach (HF) for the description of the CN decay.

In the following two sections we briefly describe the codes CEM95 and TNG and show how they can be used to make a new model code which consistently describes the whole reaction process, according to the above description.

II.1. THE CASCADE-EXCITON MODEL CODE CEM95

In CEM95 the whole sequence of the reaction process is described semi-classically in three stages. In the first stage (INC) the target nuclide is divided into spherical zones of the nuclear potential with different neutron and proton number densities. The phase space of the tracked particle is uniformly sampled using Monte Carlo techniques either for the description of its movement toward the target or inside the intermediate composite system.

The cascade model of CEM95 considers the primary particles as belonging to a degenerated Fermi gas in which all kinematic information is kept and the residual interaction is neglected. These primary particles undergo many scatterings before being absorbed or escaping. The excited particles in the different potential zones of the intermediate nucleus are able to escape unless some conditions such as the depth of the potential of the zone or the Pauli's exclusion principle preclude escape.

The initial assumption of CEM95's INC model is the description of the diagonal elements of the density operator for nuclear states, $P(E, \alpha, t)$, by means of the following master equation, [2]

$$\frac{\partial P(E,\alpha,t)}{\partial t} = \sum_{\alpha' \neq 0} \left[\lambda(E,\alpha,E,\alpha') P(E,\alpha',t) - \lambda(E,\alpha',E,\alpha) P(E,\alpha,t) \right], \qquad \textbf{(2.1)}$$

where α represents all nuclear state quantum numbers except the energy E. The time rate of change parameter $\lambda(E,\alpha,E,\alpha')$ is defined by the first order approximation of the time-dependent perturbation theory (Fermi 's Golden Rule) [3,7,8]

$$\lambda(E,\alpha,E,\alpha') = \frac{2\pi}{\hbar} \left| \left\langle E,\alpha \left| V_{scattering} E, \right| \alpha' \right\rangle \right|^2 \omega_\alpha(E), \qquad \textbf{(2.2)}$$

where $\omega_\alpha(E)$ is the density of final nuclear states and the interaction matrix element and $\lambda(E,\alpha,E,\alpha')$ is assumed to be a smooth function of the energy of the final states. It is also assumed that the distance between subsequent collisions is large enough so that the nuclear states $\left| E\alpha \right\rangle$ can be described by plane waves in the definition of the potential matrix element.

The INC model also assumes that the many-body nuclear system is dilute with short-range interactions among nucleons so that the scattering by more than two particles can be neglected. In addition, the residual correlation among the non-excited nucleons in the target and between the cascade particles and the excited nucleons in the intermediate nuclear system are neglected, so that their motion can be

considered independent of each other. With these hypotheses Eq. (2.1) can be reduced to the Boltzmann equation, which in the classical limit can be written in terms of the precise momenta and coordinates of the scattered particles,

$$\left(\frac{\partial}{\partial t}+\frac{\mathbf{p}_k}{m}\cdot\nabla_{pk}+\mathbf{F}\cdot\nabla_{pk}\right)f_k=\int\int d\mathbf{p}_k d\Omega v_{rel}\frac{d\sigma(v_{rel})}{d\Omega}\left(f_i f_j - f_k f_l\right)\,,\qquad(2.3)$$

where the function f_k is the particle distribution function for the single-particle state $|k\rangle$, $v_{rel}=|\mathbf{p}_k-\mathbf{p}_l|/m$, is the relative velocity between two colliding particles with momenta $\mathbf{p}_k$ and $\mathbf{p}_l$, and the differential cross section, $d\sigma(v_{rel})/d\Omega$, is defined in the first Born approximation.

Due to the assumption of quasi-free (independent) motion of the nuclear components, Eq. (2.3) becomes a linearized equation for the cascade particle distribution, $f^{cas}(\mathbf{r},\mathbf{p},t)$,

$$\left(\frac{\partial}{\partial t}+\frac{\mathbf{p}_k}{m}\cdot\nabla_{pk}+\mathbf{F}\cdot\nabla_{pk}\right)f^{cas}(\mathbf{r},\mathbf{p},t)=\rho^T<\sigma v_{rel}>f^{cas}(\mathbf{r},\mathbf{p},t)+Q(\mathbf{r},\mathbf{p},t)\,.\qquad(2.4)$$

Here $Q(\mathbf{r},\mathbf{p},t)$ is a source term which depends on $f^{cas}(\mathbf{r},\mathbf{p},t)$ and therefore, Eq. (2.4) defines $f^{cas}(\mathbf{r},\mathbf{p},t)$ self-consistently. The single-particle number density, ρ^T, is defined in terms of the equilibrium (Maxwellian) distribution function, $f^T(\mathbf{r},\mathbf{p})$, for the undisturbed nucleons of the intermediate nuclear system,

$$\rho^T=\int d\mathbf{p}f^T(\mathbf{r},\mathbf{p})\,.$$

Equation (2.4) is solved using the Monte Carlo method to determine the single-particle distribution function from which all other parameters can be obtained. For example, the number of particles in the cascade stage is given by

$$N^{cas}(\mathbf{p})d\mathbf{p}=\frac{1}{\sigma_i n}\int_0^R db^2\int_{r>R}dr\int_0^{t_{cas}}dt f_b^{cas}(\mathbf{r},\mathbf{p},t)d\mathbf{p}\,,\qquad(2.5)$$

where the integration is performed over all possible impact parameters b, for particles emitted from a nucleus with radius R when the time reaches the end of the cascade process t_{cas}.

The sequence of individual scatterings is then defined by considering the possibility of particle emission by the intermediate system, both prior to and after each individual scattering.

When it is not possible for more particles to escape, the INC process is finished and the residual nuclide is likely to be left in an excited state, characterized by its exciton configuration [2,9]. At this point, begins the second stage of CEM95 in which the PE model is called upon to de-excite the nuclear system through particle emission, n, p, d, t, ^{3}He, α or γ-rays, and the corresponding creation of excited residual nuclides. When the excitation energy of a residual nuclide is sufficiently low (some few MeV)

the PE mechanism becomes unnecessary and the remaining nuclide will evolve towards more complicated states, characterized by an increasing number of excitons, resulting from the residual interactions between quasi-particles, until the formation of the compound nucleus (CN). This characterizes the third stage of CEM95 in which the evaporation model (EVAP) is called upon to complete the de-excitation process.

In either the PE or the EVAP stages, the excited nucleus is described by the exciton model. The nuclear system is considered as a gas of quasi-particles (excitons) in which the residual interactions are taken into account, but the collision kinematics and the nuclear geometry are lost. This circumstance makes it difficult to describe the angular distributions of emitted particles using only the exciton model.

To exploit the advantages and avoid the disadvantages of the cascade and exciton models, CEM95 follows its own particular approach [10] by implementing a Cascade-Exciton Model in which it is possible to explain the anisotropy of angular distributions of emitted particles in a large region of incident energies, giving an improved overall description of the nuclear reaction features in comparison with the conventional cascade-evaporation model [11].

In the modified exciton model of CEM95, the process that tends to equilibrium resulting from Eq. (2.1) is identified with a discontinuous Markovian process in which each new step in the evolution of the state of the system is completely determined by its state in the previous step. The random evolution process is then simulated by the Monte Carlo technique, allowing the generalization of the exciton model to include all nuclear transitions with $\nabla n = 0, \pm 2$ (n = number of excitons), multiple emission of particles and depletion of nuclear states due to particle emission.

The equation of state (2.1) becomes,

$$\frac{dP(n)}{dt} = \Lambda(n, E) P(n, E, t) + \lambda^+ (n-2, E) P(n-2, E, t)$$

$$+ \lambda^0 (n, E) P(n, E, t) + \lambda^- (n, 2, E) P(n+2, E, t) \tag{2.6}$$

$$\sum_j \int dT \int dE' \lambda_c^j (n, E, T) P\left(n + n_j, E't\right) \delta\left(E' - \left(E - B_j - T\right)\right) ,$$

where

$$\Lambda(\alpha, E) = \sum_{\alpha'} \lambda(E, \alpha, E, \alpha') , \tag{2.7}$$

The partial transition probabilities are given by Eq. (2.1)

$$\lambda^{\Delta n} = \frac{2\pi}{\hbar} \left| M_{\Delta n} \right|^2 \omega_{\Delta n}(p, h, E) , \tag{2.8}$$

and the rate per unit time of emission of ν-particles $\Gamma_\nu(n, E)$ is estimated with the help of the principle of detailed balance, [12]

$$\Gamma_\nu(n,E) = \int_{V_\nu^c}^{E-B_\nu} \lambda_\nu^c(n,E,\varepsilon_\nu)d\varepsilon_\nu \; , \tag{2.9}$$

where,

$$\lambda_\nu^c(n,E,\varepsilon_\nu) = \left(\frac{2s_\nu+1}{\pi^2\hbar^3}\right)\mu_\nu A_\nu(n)\sigma_\nu(\varepsilon_\nu)\varepsilon_\nu \frac{\omega_\nu(p-1,h,E-B_\nu-\varepsilon_\nu)}{\omega(p,h,E)} \; . \tag{2.10}$$

where ε_ν is the kinetic energy of the emitted particle, s_ν is its spin, B_ν is the binding energy of the emitted particle in the decaying nuclide, V_ν^c is the Coulomb barrier before emission, and μ_ν is its reduced mass relative to the rest of the nuclear system. The factor $A_\nu(n)$ ensures that the emitted particle is of type ν and can be directly calculated within the model with the help of the Monte Carlo method.

The CEM95 exciton model makes the usual assumptions about the single-particle level density, $\omega(p, h, E)$, using the equidistant nuclear level scheme and the results of Williams and Ribansky *et al.* [8,13] to correct the level density for the effects of the Pauli's exclusion principle and the indistinguishability of excitons of the same type. This leads to the explicit expressions for the cross section average term [12],

$$\left\langle \sigma(v_{rel})v_{rel}\right\rangle = \left(\frac{\pi V_{\text{int}}}{\hbar}\right)|M|^2 \frac{g[gE-C(p+1,h+1)]}{n+1}\left[\frac{gE-C(p+1,h+1)}{gE-C(p,h)}\right]^{n-1} , \tag{2.11}$$

where g is the constant single-particle density of levels, V_{int} is the interaction volume and the average on the left hand side is calculated over all excited states allowed by the exclusion principle. The factor

$$C(p,h) = \frac{1}{4}\left(p^2+h^2+p-3h\right),$$

is the exclusion principle correction term for the level density function. Equation (2.11) is used to directly estimate the average matrix element $|M|^2$ within the model and is in good agreement with the widely used parameterization of Kalbach [2,14].

In general, the model considers three independent components to define each experimentally measured parameter. For the particle spectrum the definition is,

$$\sigma = \sigma_{in}\left[N^{cas}(\mathbf{p}) + N^{pre}(\mathbf{p}) + N^{eq}(\mathbf{p})\right], \tag{2.12}$$

where the reaction cross section σ_{in} is calculated directly within the cascade model.

In the above expression N is the number of particles in each stage of the total process. Dividing each number by the total sum results in the corresponding cross section. For example, the contribution corresponding to the cascade stage is

$$\sigma^{cas} = \sigma_{in}\frac{N^{cas}(\mathbf{p})}{\left[N^{cas}(\mathbf{p}) + N^{pre}(\mathbf{p}) + N^{eq}(\mathbf{p})\right]} \; .$$

N^{cas} (**p**) is given by Eq. (2.5) and the pre-equilibrium and equilibrium components of the inclusive spectrum of particles of type ν are given by,

$$N^{pre}(\mathbf{p})\,d\mathbf{p} = \int_{t_{cas}}^{t_{eq}} dt \sum_n \lambda_\nu^c(n,E,\varepsilon_\nu) P(n,E,\varepsilon_\nu) \frac{\partial(p,\Omega)}{\partial(\varepsilon_\nu,\Omega)} F(\Omega)\,d\Omega\,d\varepsilon_\nu \,, \qquad (2.13)$$

and

$$N^{eq}(\mathbf{p})\,d\mathbf{p} = \int_{t_{eq}}^{\infty} dt \sum_n \lambda_\nu^c(n,E,\varepsilon_\nu) P(n,E,\varepsilon_\nu) \frac{\partial(p,\Omega)}{\partial(\varepsilon_\nu,\Omega)} F(\Omega)\,d\Omega\,d\varepsilon_\nu \,. \qquad (2.14)$$

The transition from the cascade stage to the pre-equilibrium stage is determined by the relative departure between the imaginary part of the optical potential calculated from the excitation functions obtained with the cascade model, W_{mod}, and the optical potential obtained from the experimental data, W_{exp}. The proximity parameter, D, is defined as

$$D = \left| \frac{W_{mod}(r) - W_{exp}(r)}{W_{exp}(r)} \right| \,,$$

and the cascade process is described with $D \approx 0.3$. The value of D was determined from the analysis of the experimental data concerning fast backward emitted protons [2,15].

CEM95 neglects the production of complex particles in the INC stage of the reaction. Only in the PE stage is the possibility of complex particles formation taken into account to produce fast emitted complex particles. The formation of complex particles at low energy is considered in the EVAP stage. The possible complex particle types considered by CEM95 are d, t, ^{3}He and α.

II.2. THE MODEL CODE TNG

The model code TNG utilizes the optical model (OM) in connection with the formalism of Hauser-Feshbach (HF) [16] and a PE model with angular momentum conservation to obtain angular distributions for the outgoing spectrum. It also utilizes the double fission barrier theory of Lynn [17] and a giant-dipole resonance model for the calculation of ϒ-ray strength functions with width fluctuation corrections for the discrete levels as well as the continuum (region described by the level-density function).

The TNG model is based on a formalism that consistently unies statistical (HF) and pre-equilibrium (PE) models [3,18]. This formalism uses a modified exciton model for the description of precompound emission, which automatically reduces to the usual evaporation formula after the equilibrium has been reached. A detailed description of the TNG model can be found in Ref. [18] and the original formulation in Ref. [3]. We reproduce only its most important aspects, to compare with CEM95's model presented in the previous section.

In TNG the calculation of the decay spectra is characterized by integrations of the equation of state along the intervals [0, T], for the pre-equilibrium emission, and [T, $\propto$], for the CN emission, where T is the time interval necessary for the equilibrating system to reach the CN stage.

If $P_v(n)$ is the occupation probability distribution of single-particle states filled with particles of type v, in intermediate nuclear states with exciton number n, then its time rate of change is defined by a master equation analogous to Eq. (2.6) [3,8],

$$\frac{dP_v(n)}{dt} = \left[P_v(n-2)\left(\frac{p-1}{p}\right) + \frac{f_v(p)}{p}P(n-2) \right]\lambda^+(n-2) +$$

$$P_v(n+2)\lambda^-(n+2) - P_v(n)\left[\lambda^+(n) + \lambda^-(n)^+ \int_0^{(E-B_v)} X_v(n,\varepsilon_v)d\varepsilon_v \right],$$

(2.15)

where p is the number of excited particles, E is the excitation energy of the decaying nuclide, ε_v is kinetic energy of the emitted v-particle and B_v is its binding energy before emission.

The functions $\lambda^+(n)$ and $\lambda^-(n)$ are the internal rates of transition from nuclear states with initial exciton number n to states with final exciton number $n+2$ and $n-2$, respectively. These functions describe a steady equilibrium state of the excited nuclear system and do not include the emission process.

The function $f_v(n)$ is the probability of finding particles of type v in a newly excited n-excitons nuclear state, resulting from the excitation of one v-particle (and one v-hole) on a nuclear state with $(n - 2n_v)$-excitons, where n_v is the total number of excitons associated with the creation of a particle of type v.

Therefore, the function $f_v(n)$ describes a perturbed situation which is complementary to the steady-state described by $P_v(n)$, λ^+ and λ^- but this perturbation is assumed to be weak enough so that the nuclear steady-state is not altered.

The consistency between PE and EVAP mechanisms in the above description of the equilibrating process lies on the specific definition of a master equation for each component, $P_v(n)$, of the emission spectrum. This avoids the use of *ad hoc* probability parameter to describe the relative presence of v-type particles among the total p excited ones for nuclear states with given n and E and permits the definition of this parameter in a time-dependent way within the model itself [18,19].

The time rate of transition between single-particle excited states in the intermediate nuclear system, λ, is given again by the Fermi's Golden Rule [20],

$$\lambda = \frac{2\pi}{\hbar}\sum_f \left|\langle i|V_{residual}|f\rangle\right|^2 \delta(\varepsilon_f - \varepsilon_i),$$

(2.16)

where $|i\rangle$ and $|f\rangle$ are the initial and final nuclear states, respectively, with energies ε_i and ε_f, and the sum over final states include all possible transitions compatible with the residual interaction, the conservation laws, and Pauli's exclusion principle.

The model assumes that the residual interaction does not depend strongly on the final states so that its mean value, $|i\rangle |V_{residual}|f\rangle|^2$, can be factored and the above expression can be rewritten as,

$$\lambda^{\Delta n} = \frac{2\pi}{\hbar}M_{\Delta n}^2 Y,$$

(2.17)

where $M_{\Delta n}^2$ is the average square matrix-element for two-body interactions between a specific initial state and any possible final state, compatible with the given variation of the exciton number, Δn. The residual interaction is assumed to be of two-body type. Therefore, the variation in exciton number between initial and final single-particle (sp) states is $\Delta n. = \pm 2, 0$. As in the CEM95 model, in the derivation of expression (2.14) the dependence of the interaction matrix element, $M_{\Delta n}^2$, on Δn is neglected.

The parameter Y measures the total number of available final states for possible transitions, for a given excitation energy interval $[E,E+dE]$. Assuming an equidistant level spacing model for the sp-energy spectrum, with distance between levels g and the conditions

$$p << \sqrt{gE} \quad \text{and} \quad h << \sqrt{gE},$$

the density of final sp-states of an n-exciton nuclear system, Y is given by Ref. [21],

$$Y(n,E)=\omega(n,E)=\frac{g(gE)^{n+1}}{p!h!(n-1)!}.$$
(2.18)

Equations (2.17) and (2.18) permit the calculation of $\lambda^+(n)$ and $\lambda^-(n)$ in a phenomenological way with explicit expressions which take into account Pauli's exclusion principle, according to Williams' formulation [13,3].

In equation (2.15) the function X_v measures the rate per unit time of the emission of particles of type v from nuclear states, defining a decrease of the occupation probability for a given exciton-number which is estimated using the principle of detailed balance [18,12]

The total pre-equilibrium plus equilibrium emission spectra can be written as

$$\sigma_v^{total}(\varepsilon_v)d\varepsilon_v =\left(\frac{2s_v+1}{\pi^2\hbar^3}\right)\mu_v\sigma_v(\varepsilon_v)\varepsilon_v d\varepsilon_v$$
$$\times\left[\sum_p\frac{\omega_v(p-1,U)}{\omega(p,E)}\int_o^T P_v(p,t)dt+\sum_p\omega_v(p-1,U)\int_T^\infty\frac{P_v(p,t)dt}{\omega(p,E)}\right],$$
(2.19)

where the various symbols have the same definition as in Eq. (2.9), and σ_{CN}, analogous to σ_{in} in Eq. (2.12), is the cross section for formation of the CN. Here the number of holes is assumed to vary by the same amount as the number of particles in the equilibrating process and, therefore, the sum over the number of particles represents a sum over the exciton number varying in steps of two units.

Another important aspect of the exciton model used in TNG is the conservation of the angular momentum in a form compatible with the Hauser-Feshbach formula, which avoids arbitrary assumptions about the spin populations in the PE stage.

To define the spin distribution for pre-equilibrium states the TNG model takes into account the spin direction in the principle of detailed balance and decomposes the emission rate, X_v, into its spin-dependent components [12,22],

$$X_\nu(n,J,I,E,\varepsilon_\nu)\,d\varepsilon_\nu = \frac{1}{2\pi\hbar}\sum_{s'l'} T^J_{\nu s'l'}(\varepsilon_\nu)\,d\varepsilon_\nu\,\frac{\rho_\nu(p-1,I,U)}{\rho(p,J,E)}\ , \tag{2.20}$$

where the diverse parameters are

parameter	description
$T^J_{\nu s'l'}$	optical-model transmission-coefficient,
J	total spin of the reacting system,
I	spin of the residual level,
s'	spin of the emitted particle ν,
l'	orbital angular momentum of the emitted particle ν,

and the spin-dependent level density, $\rho(p, h, J, E)$, is given by its relation to the single-particle state density, $\omega(p, h, E)$, by the expression

$$\rho(p,h,J,E) = \omega(p,h,E)R(n,J)\ ,$$

where the distribution of spins of the excited system is in Ref. [23],

$$R(n,J) = \frac{(2J+1)}{2(2\pi)^{1/2}\,\sigma^3(U,n)}\exp\left[-\left(J+\frac{1}{2}\right)^2\Big/2\sigma^2(U,n)\right],$$

and the spin-cutoff parameter, $\sigma^2(U, n)$, is given by a numerically fitted expression of the formula of Ignatyuk and Sokolov [3,24],

$$\sigma^2(U,n) = (\ln 4)\left(\frac{n}{n_c}\right)\left(\frac{U-U_{th}}{U}\right)^x\ , \tag{2.21}$$

where the exponent is a function of (n/n_c), given by,

$$x = -0.413 + 1.08\left(\frac{n}{n_c}\right)^{1/2} - 0.226\left(\frac{n}{n_c}\right),\tag{2.22}$$

and the minimum excitation energy, U_{th}, in the uniform pairing model [25] can be approximated by a simple numerical fit [3],

$$\frac{U_{th}}{C}=\begin{cases}3.23(n/n_c)-1.57(n/n_c)^2 & \text{if}\quad (n/n_c)\leq0.446\\1+0.627(n/n_c)^2 & \text{if}\quad (n/n_c)\leq0.446\end{cases}, \tag{2.23}$$

where n_c is the most probable quasi-particle number at the critical temperature given by

$$n_c=2gT_c\ln2=\left(\frac{\ln16}{3.5}\right)g\Delta_0 , \tag{2.24}$$

where Δ_0 is the average pairing-gap in the ground-state determined by the following dependence with the nuclear mass number [24],

$$\Delta_0=\frac{12}{\sqrt{A}} , \tag{2.25}$$

and C is the so called condensation energy which measures the lowering of the ground-state energy of a many-body system due to the formation of a boson condensate of Cooper pairs [26]. In the uniform pairing model the condensation energy is given by

$$C=\frac{g\Delta_0^2}{4} . \tag{2.26}$$

For excitation energies below U_{th} the spin cut-off parameter vanishes and, consequently, the level-density function also vanishes. Therefore, no composite nucleus with excitation energy less than U_{th} can exist.

The pairing gap for the excited system, $\Delta(U, n)$, can also be approximated by the following simple fitted function,

$$\frac{\Delta}{\Delta_0}=\begin{cases}0.996-1.76(n/n_c)^{1.60}(U/C)^{-0.68} & \text{if}\quad U\geq E_{ph} ,\\0 & \text{if}\quad U<E_{ph} ,\end{cases} \tag{2.27}$$

where U is the excitation energy and E_{ph} is the energy of the pairing phase transition [19], that is, the minimum energy necessary to set up a system of p particles and h holes, taking into account the pairing-energy gap in the sp-levels close to the Fermi surface,

$$E_{ph}=C\left[0.716+2.44(n/n_c)^{2.17}\right]\quad\text{for}\quad n/n_c>0.446 . \tag{2.28}$$

The cross-section formula that accounts for both the compound and precompound effects is given by,

$$\sigma_v(E,\varepsilon_v)d\varepsilon_v=\left(\frac{\lambda_v^2}{4\pi}\right)\sum_{J\pi sl}\left(\frac{g_J T_{vs'l'}^J}{D_{J\pi}}\right)\sum_p X_v(n,J,I,E,\varepsilon_v)d\varepsilon_v\int_0^\infty P_v(p,J,t)dt , \tag{2.29}$$

where λ_v is the De Broglie wave length, given by,

$$\lambda_\nu = \frac{\hbar}{\mu_\nu \nu_{rel}} ,$$

where ν_{rel} is the velocity of the relative motion of collision partners and μ_ν is the reduced mass of the particle-target system. In Eq. (2.29), the quantity $D_{j\pi}$ is given by,

$$D_{J\pi} = \sum_{\nu I \pi p} \int_{\varepsilon_\nu} X_\nu d\varepsilon_\nu \int_0^\infty P_\nu dt , \qquad (2.30)$$

and was introduced here to ensure that the quantity inside the brackets has the meaning of a branching ratio. $D_{J\pi}$ is similar to the factor $\omega_\nu(p - 1, U)/\omega(p, E)$ in Eq. (2.10).

A useful approximation to deal numerically with the above expression is

$$\frac{P_\nu(n,J,t)}{\omega(nJ,E)} = \frac{P_\nu(n,t)}{\omega(n,E)} .$$

This approximation enables the direct use of Eq. (2.19) and describes the assumption that all spin states in the composite system are equally populated during the equilibrating process.

Noting that the transmission coefficients are independent of the particle-hole indices, the cross section formula becomes

$$\sigma_\nu(E,\varepsilon_\nu)d\varepsilon_\nu = \left(\frac{\lambda_\nu^2}{4\pi}\right) \sum_{J\pi sl} g_J T_{\nu s'l'}^J \frac{d\varepsilon_\nu}{D_{J\pi}} \sum_{s'l'} T_{\nu s'l'}^J \Omega_\nu(I,E,U) , \qquad (2.31)$$

where

$$\Omega_\nu(I,E,U) = \sum_p C_\nu(p,E)\rho_\nu(p-1,h,I,U) ,$$

with

$$C_\nu(p,E) = \int_0^\infty \frac{P_\nu(p,h,t)}{\omega(p,h,E)} dt ,$$

which is the basis for cross-section calculation in the TNG model.

If the instantaneous equilibrating process is assumed, Eq. (2.31) reduces to the usual Hauser-Feshbach formula, which amounts to replacing the integral $\int_0^\infty P_\nu(p,h,t)dt$ by $\omega(P,h,E)$ and the sum $\sum_p \rho_\nu(p-1,h,I,U)$ by the conventional level density, $\rho_\nu(I,U)$. For a finite time equilibrating process, Eq. (2.31) explicitly accounts for the spin distribution in the pre-equilibrium stage.

Therefore, the pre-equilibrium and the Hauser-Feshbach parts of the model are defined in a consistent way.

II.3. THE NEED FOR A QUANTUM MECHANICAL DESCRIPTION

A major problem in the INC-PE-EVAP sequence described in Sect. II.1 is in the reaction process a dominant number of the residual nuclides is excited to less than 20 MeV. To check the continuation line. In this region the emitted particles cannot be treated as semi-classical, but must be treated as waves. Therefore, quantum-mechanical models are necessary for the description of these emergent particles to get a reasonably precise prediction of the radio-nuclide yields. This is especially important for the radio-nuclides of longer life in waste transmutation technologies.

The solution of this problem, translated into model codes, consists of the replacement of the semi-classical models in low energies with the corresponding quantum-mechanical models. However, to implement this a series of problems must be solved.

The non-microscopic EVAP model used in HETC and CEM95 cannot calculate the cross- sections for the excitation of discrete levels and cannot account for the effects resulting from the spins and parities of single-particle levels. The HF model can do this and TNG makes maximum use of the known discrete levels of the various residual nuclides by allowing a continuous overlap of the discrete-level region and the continuum region.

The most recent version of evaluated neutron cross-section files in the U. S. (ENDF/B-VI), contains discrete-level information that can be used for precise calculation of the cross sections for exciting each discrete level of the residual nuclide and the cross sections of γ-ray transitions between each level and all others below it. This type of information can only be generated by analyzing experimental data with HF codes such as TNG. This discrete-level information is available for 26 isotopic calculations which were performed with the TNG code and contributed to ENDF/B-VI by ORNL. This detailed information is often needed by data users and will also be available from the calculations performed with the new CETNG code.

For energies somewhere above 40 MeV, either for the incident particle energy or for the excitation of the residual nuclide, the INC and the PE parts of CEM95 are adequate. The comparison of calculated results with experimental data has been extensive [2] and has demonstrated its capability for simulating direct reactions and multiple-particle emissions. In the energy region below 40 MeV the discrete levels become too important to be ignored and the TNG calculation is preferred over the CEM95 calculation. This is clearly illustrated, for example, in Figures 1 and 2 where we show the production cross section for ^{55}Co and ^{56}Co, respectively, with *p*-induced reactions in elemental Fe.

On the other hand, because TNG is a more detailed model code than CEM95, it demands more computing capabilities and, therefore, should be used for the smallest possible energy region. The energy boundary, below which TNG is used, is entered as an input parameter to the new code. Assume that 20 MeV is the boundary between semi-classical and quantum-mechanical physics for the emitted particle. Then we may use TNG for incident energies between 1 and 20 MeV and use the new code (CETNG) for energies above 20 MeV. With respect to the excitation energies of the intermediate nuclear system, the semi-classical to quantum-mechanical boundary in this case is 20 MeV plus the binding energy of the emitted particle in the residual nucleus. Assume that this energy is 27 MeV for a given final channel.

For an incident energy of 50 MeV the new code CETNG will be used and will call the INC model first. Because this incident energy is very low for INC, it will be quickly finished. PE will then be called and start the de-excitations from the highest energy downward. PE proceeds down to an excitation energy less than 27 MeV, where it calls TNG to switch to quantum-mechanical physics to complete the remaining de-excitation. The additional residual nuclides created are likely to be excited to energies well below 27 MeV. Therefore, for incident energies close to the boundary (20 MeV), TNG is still dominant and the resulting data will vary smoothly from the 20 MeV data. All discrete-level data will be continuous across the boundary.

On the other hand, for an incident nucleon energy of 150 MeV, CETNG will call INC which will perform many calculations before calling PE. Therefore, the resulting data will have significant direct-reaction and multiple-particle components of the INC model. TNG will still be important because a large number of excited nuclides in TNG's energy range will be created, all dependent on TNG for further de-excitation and creation of additional residual nuclides.

In summary, in CETNG the EVAP model of CEM95 was replaced by TNG and the low-energy part of the CEM95's PE model, being semi-classical, was also replaced by the quantum mechanical PE model of TNG.

III. COMPARING RESULTS

In the first step of the development of CETNG we compared the calculated results of CEM95 with TNG and experimental data in the 20 to 40 MeV region, mainly for the (*n, xn*) and (*p, xn*) cross sections and the out-going particle angular spectra for a few selected targets.

We already had TNG results for incident neutron energies below 20 MeV for a number of targets, including discrete-level information. CEM95 was run for one of the targets at 20 MeV to compare with TNG data. The resulting reaction cross sections disagreed, some of them significantly, and the discrete-level information and γ-ray production cross section available from the TNG results were non-existent in the CEM95 results. Similar comparisons for a wider range of energies and reactions were performed.

These comparisons highlighted the strengths and weaknesses of each code in the overlapping energy range and helped to determine the additional efforts that were needed. The energy below which TNG could be loaded and the excitation energy at which CEM95 should call TNG could be estimated from these comparisons. This energy is expected to decrease with increasing mass number.

III.1. AUTOMATIC GENERATION OF INPUT FILES

To make a detailed comparison between CEM95 and TNG, some simple programs have been developed for the automatic generation of simplified TNG input files, fort.60 and fort.63, that can be used when a large number of successive particle emissions is considered in the reaction sequence. Some simplifications were introduced at this initial stage to facilitate the implementation of the connection between TNG and CEM95 in the energy range below the intranuclear cascade threshold. Increasingly complex reactions sequences are planned for the next stage of the development of CETNG, in particular, with the inclusion of *d*, *t* and ^{3}He as emitted particles in the TNG spectra.

In Table I , the constraints used on TNG input data are shown

---

Table I - Simplified Automatic TNG Input

Two possible incident particles: *p, n*

Three possible emitted particles (besides radiative capture and fission reactions): *p, n*, α

Optical Model parameters given by adequate default options for the different emitted particles.

Cross-section for direct excitation of the residual nucleus levels was neglected.

The reaction energy was fixed (but can be altered or stacked afterwards)

For protons and neutrons, the global optical potential used in the LA150 library, recently developed by Chadwick *et al.* [1], was introduced as an option in TNG and was used in this work. For α particles the potential of McFadden and Satchler [27] was used.

Neglecting the cross section for direct excitation of the residual nucleus levels implies an approximation when performing calculations with CETNG in the region where both TNG and CEM95 contributions are important. In this case, we can use DWBA calculations to add direct components to TNG input as correction factors.

Some minor modifications were introduced in TNG to enable it to calculate cross sections for reactions with up to 8 emitted particles which are needed for reactions with higher energy thresholds. To permit an easier automation of the various steps involved in the description of a reaction where many particles are emitted, some variables, such as the existence of fission processes, were neglected. The series of multi-particle emission reactions in the post-binary stage (fort.63) was defined in a systematic way, considering all possible particle emissions up to a maximum of 8 emitted particles (only *p, n* and α emissions were considered in this work).

In Table II the modifications introduced in TNG to make it consistent with CEM95 are shown. The available experimental data (see Refs. [29] and [30]) were used to automatically define the level schemes and decay branching-ratios as a function of the nuclear mass number (A) and charge (Z).

The function that determines the mass defect and the reaction-Q for the various nuclei, in terms of the mass and charge number, has a phenomenological dependence on the parameters of shell and pairing corrections S(Z)+P(Z) and S(N)+P(N) of Cameron [31], or the analogous parameters $\Delta M(N)$ and $\Delta M(N)$ of Malyshev's book [32].

CEM95 has a level-density model suitable for excitation energies from about 7 MeV, the average neutron binding energy, up to several GeV. The model accounts for odd-even effects and the shell structures near the neutron binding energy and allows the shell structures to disappear above 100 MeV. The model ignores the low-energy level density defined by the discrete levels. On the other hand, TNG has a level-density model that takes the available discrete levels into account, and, hence, works better in the low energy range. In the initial stage of this project the TNG model did not have theCEM95 feature of forcing the shell structures to disappear at high energies and, therefore, it under-predicted the number of levels for excitation energies above 20 MeV. Presently, the addition of the Mengoni-Nakajima model treats this level-density feature in TNG [33].

Table II - Modifications of TNG Code

The number of emitted particles in each reaction was increased to a maximum of 8.

The level schemes and decay branching-ratios for the various nuclei in the reaction cascade were automatically generated as a function of the nuclear mass number and charge. These data were used in both input files of TNG.

The reaction-Q in each step of the cascade process was calculated with the same function used in CEM95.

The same level-density and OM sets of parameters were used in both codes.

In CETNG the good physical features of TNG and CEM95 were combined so that the level densities in both codes are consistent over the whole energy range. This reduced the discrepancies between the two codes and resulted in improved versions of both. More specific definitions concerning the construction of CETNG are described in Ref. [28] along with some numerical results and a detailed explanation of the method used to combine the calculations of TNG and CEM95 in the PE region.

III.2. RESOLVING PHYSICAL INCONSISTENCIES

The most difficult part of the solution of physical inconsistencies between the two codes is that CEM95 is semi-classical while TNG is spin and parity dependent; that is, TNG solves one partial wave at a time for the calculation of cross sections. Therefore, TNG needs the definition of the spin distribution of the residual nucleus as a function of the mass number and the excitation energy for the calculation of level-densities and transmission coefficients in the Hauser-Feshbach formalism.

A simple numerical solution is to run TNG first for some incident energies and some targets and to parameterize the resulting spin distribution as a function of the incident energy, excitation energy, and mass number. The initial spin distribution functions have the same form as those used in the TNG level-density model, but have a different mass and energy dependence for the spin cutoff parameters. Another solution results from using the distribution calculated by TNG directly for lower incident energies, assuming that the resulting function is valid in the extended region where CEM95 cross-section calculations are more important than that of TNG. In all cases, the parity distributions are initially taken as half positive and half negative. Therefore, every time TNG is called by CEM95 to make the calculation, TNG knows what spin and parity distributions should be used for every residual nuclide and all of its excitation energies.

In the next section the simple model used for the spin distribution function is shown. It is expected to provide meaningful results for all mass numbers and energies.

III.2.1. Spin Distribution

To find the spin distribution function, a systematic analysis of the dependence of the number of excited residual nuclei with the nuclear spin, as a function of the nuclear mass (A), excitation (E_{ex}), and incident (E_{inc}) energies, was performed.

A simple expression for $R(J)$, the spin distribution function, was derived by Bethe [6]

$$R(J) = \frac{(2J+1)}{2\sigma^2} \exp\left[\frac{-(J+1/2)^2}{2\sigma^2}\right], \tag{3.32}$$

where the spin cut-off σ^2 is given by an expression from Gilbert-Cameron [23],

$$\sigma^2 = \left(\frac{6}{\pi^2}\right) a <m^2> T, \tag{3.33}$$

with the following definitions,

$$T = \sqrt{\frac{E - U_0}{a}} \qquad \text{(the nuclear temperature)}, \tag{3.34}$$

$$U_0 = \frac{12 n_s}{\sqrt{A}} \qquad \text{(then pairing correction)}, \tag{3.35}$$

where n_s is the nuclear symmetry factor (=0 for odd-odd nucleus, 1 for odd-even and even-odd nucleus, and 2 for even-even nucleus) and the average square of the magnetic quantum number for single-particle states was taken in accordance with the Generalized Superfluid Model (GSM) [24], with parameterization of Mengoni and Nakajima [33],

$$<m^2> = 0.24 A^{2/3}, \tag{3.36}$$

and the expression for the Fermi gas parameter as a function of A was taken simply as [35]

$$a = \frac{A}{8}.$$

For low energies, the phenomenological Mengoni-Nakajima level-density model was used in which the Fermi parameter also has an excitation energy dependence as follows,

$$a(U, A) = \tilde{a}(A)\left\{1 + \frac{[f(U')S]}{(U')}\right\}, \tag{3.37}$$

where S is the shell correction for the nuclear binding energy according to the formulation of Myers and Swiatecki [34], U' is the effective nuclear excitation energy, $f(U')$ is an exponential function of U' and $\tilde{a}(A)$ is the assymptotic value of a at high excitation energy. The function f determines the energy behavior of a for lower excitation energies. In the original Gilbert-Cameron formulation the parameter a had a simple linear dependence on the total shell correction S as a function of the nuclear charge and mass.

The Mengoni-Nakajima formulation implemented in TNG is further improved by a continuous match to the discrete single-particle level structure, in accordance with the Gilbert-Cameron approach.

For lower energies up to about 80 MeV, a replacement procedure can be devised to account for spin and parities, which directly uses the TNG results in the low energy region (see details in Ref. [28]). In this case the excitation spectra calculated in TNG with excitation energies above the low energy threshold are replaced by small arbitrary cross section values to keep CEM95's results for the cross section calculations and to force TNG to extend the spin parity calculations up to 80 MeV.

The extension of TNG calculations to energies above 80 MeV is not yet possible, because the description of excited states with energies in this region is not yet implemented. In addition, the independent definition of a distribution function for this energy range is not simple because the procedure must be automated as part of CETNG. This part of the calculation must be reprogrammed by analyzing each calculated spin distribution and validating it with the use of models already implemented in TNG to achieve a consistent description with the low energy range.

Therefore, as a first step to define the spin distribution in the region above 80 MeV, a function which has the adequate *average* properties as a function of the energy and atomic mass has been examined. The spin cut-off σ^2 was parameterized as a function of A and E with parameters p_1, p_2, and p_3 as follows,

$$\sigma^2 = p_1 \, A^{p_2} \, E^{p_3} \ .$$

and the parameters, p_1, p_2, and p_3 are varied with the initial values,

$$p_1 = 0.051584, \quad p_2 = 7/6 \quad \text{and} \quad p_3 = 1/2 \ .$$

The fitting procedure is a self-consistent least squares method, following the systematics developed by G. M. Wharton and D. K. Olsen [36], and the parameters are tted against the results of TNG for a large set of reactions for incident energies from 20 to 50 MeV and considering all resulting residual nuclei excitation energies generated by TNG's model. Two target nuclei were used, ^{56}Fe and ^{202}Hg.

Different functions with dependence on the number of emitted particles, incident energy (E_{inc}), excitation energy of the residual nucleus (E_{ex}), and the mass number of the residual nucleus were obtained. It was noted that E_{inc} and E_{ex} cause the spin distribution function to vary in opposing ways, and that no simple function could be found that properly described all its variations. Therefore, for high energies it was concluded that a function qualitatively correct for all possible energies and mass numbers and simple enough to be used as a high- energy option of CETNG is adequate. A very simple function that satisfies these conditions with respect to E_{inc} and A is

$$\sigma^2 = A^{0.6} \, (E_{inc} - 27.)^{0.37} \ . \tag{3.38}$$

Despite its simplicity, this function produces good qualitative average spin distributions for all analyzed incident energies and mass numbers between the Fe region ($A=56$) and the Hg region ($A=202$). A more sophisticated model will be deferred while a clear theoretical explanation cannot be given, particularly with respect to the complementary behavior of the spin distribution with E_{inc} and E_{ex}.

A more detailed statistical analysis of the excited residual nucleus levels and the corresponding spin distributions for energies above 80 MeV is being planned for a future work.

IV. RESULTS AND CONCLUSION

Performing a cross-section calculation with the new code for a given target and incident energy, e. g., between 1 and 200 MeV, requires one to start with the new CETNG code. CETNG calls the INC model. The INC model calls its own PE model, and finally runs the improved TNG for incident-particle energies between 1 MeV and E_c. E_c is an input value usually taken between 20 and 40 MeV. In these initial runs, the global spin and parity distributions defined in the previous section are refined for a small mass number range suitable for the given target. As explained earlier, TNG will still be dominant for incident particle energies a little higher than E_c, so the transition from TNG to the new code is expected to be smooth for all calculated data, including the discrete-level data.

In the new code, the EVAP model of CEM95 was replaced by the improved TNG version. The excitation energy at which TNG is called is much higher than the energy at which the original EVAP was called because TNG has a quantum mechanical PE model that works very well up to 80 MeV. The initial results of CETNG show that the new code gives better results than either CEM95 or TNG in the 5 to 80 MeV range [28].

Comparisons of CETNG calculated cross sections for proton induced reactions on natural Fe with the measurements of Michel *et al.*[37], for incident energies E_{inc} up to 2.6 GeV, are discussed in Ref. [28]. Some results of CETNG code are shown in Fig. 3 . In all calculations, either in Ref. [28] or in this paper, the contributions from ^{57}Fe, ^{56}Fe and ^{54}Fe have been multiplied by 0.022, 0.92 and 0.058, respectively, to account for their isotopic abundances. In the results of Ref. [28] TNG was used for incident energies below 40 MeV and CETNG for higher energies. The CETNG calculations are still preliminary because the model is being refined. The model parameters used were somewhat arbitrary and were taken from previous default options of CEM95 and TNG.

Figures 1 and 2 show the results for $(p,2n)$ and (p,n) cross sections, respectively, for elemental Fe for energies from the activation threshold up to 200 MeV. In both cases the TNG calculation shows good agreement with the experimental data, from the activation threshold up to about 45 MeV, and CEM95 has a reasonably good agreement for E_{inc} above 25 MeV and 50 MeV, for the $(p,2n)$ and (p,n) reactions, respectively, being an average of 35% larger in the first case and 35% smaller in the second. In the 30 to 45 MeV region, TNG and CEM95 results are close, but TNG is clearly more accurate than CEM95 in this energy range.

Both calculations show a smooth transition from low to high energy and the new results from CETNG show significant improvement in the region below 100 MeV in comparison with the independent results from TNG and CEM95 [28]. In Fig. 4 the calculation of the $(n,2n)$ cross section for ^{56}Fe shows the same smooth transition, but the experimental data is too sparse for a more detailed comparison.

Figure 5 shows the cross section for the production of ^{51}Cr with *p*-induced reactions in elemental Fe. Our calculations identify three peaks in the experimental ^{51}Cr production data. There is a 45 MeV peak which results from the ^{56}Fe (p,pn) reaction, another non-sharp peak at 90 MeV which results from ^{56}Fe $(p,3p3n)$, and there is also a small contribution from the ^{54}Fe$(p,3pn)$ reaction. The measured data for ^{51}Cr below 30 MeV is from the ^{54}Fe$(p,p$ ^{3}He$)$ reaction that cannot be treated in the present version of TNG, but will be allowed in CETNG.

For ^{51}Cr production the TNG calculation shows good agreement with the experimental data from the activation threshold to about 60 MeV. Above that,TNG calculations do not agree with the experimental data. Conversely, CEM95 does not agree with the experimental data for energies below 120 MeV but

gives a good account for E_{inc} above 120 MeV to 250 MeV, with less than a 25% average deviation in this region. Both calculated data disagree with the experimental points in the 60 to 120 MeV region. CEM95 reasonably predicts the magnitude of the cross section in this region, but the curvature of the calculated curve is very different from the experimental data. In this case, CETNG results (see Fig. 3) indicate an improvement for very high energies (above 500 MeV) but the peak at about 90 MeV is still not predicted. It is likely that some improvement can be achieved with the adoption of better optical parameters, such as those obtained by Koning *et al.* [38], which give a good description of this reaction.

Figures 6 and 7 show the cross sections to produce ^{52}Mn and ^{54}Mn, respectively, with *p*-induced reactions in elemental Fe. The ^{52}Mn production has a large contribution due to the *(p,n)* reaction in ^{56}Fe, with a peak around 33 MeV, and another high-energy peak due to (*p*,3*n*2*p*) reaction in ^{56}Fe. There is still a small contribution from the ^{54}Fe(*p*,*n*2*p*) reaction, with a peak at 40 MeV. ^{54}Mn production results from the (*p*,*n*2*p*) reaction in ^{56}Fe and two smaller contributions from the (*p*,2*n*2*p*) and (*p*,α) reactions in ^{57}Fe. The last reaction is responsible for the low energy peak around 10 MeV. For both reactions TNG's calculation shows good agreement with the experimental data from the activation thresholds to about 50 MeV.

For ^{52}Mn production, CEM95 misses the experimental results for energies above 80 MeV but give good results in the lower energy regions, close to TNG's estimate. In this case, the results obtained with CETNG are greatly improved mainly for high energies but the experimental peak near 75 MeV still cannot be reproduced. The solution for this problem is probably similar to the analogous one in the ^{51}Cr production case, because the OM set of parameters of the LA150 library of Ref. [1] are used, which does not properly describe the 60 to 100 MeV region for this reaction.

For ^{54}Mn production CEM95 results are in excellent agreement with experimental data from about 60 to 250 MeV and the combined results from TNG and CEM95 is reasonable for all energies between the activation thresholds and 250 MeV. The calculations with CETNG show improved results in the region of transition from TNG to CEM95 data around 50 MeV [28].

Figure 8 shows the nonelastic *n*-induced cross sections calculated with CEM95 and TNG for elemental Fe for incident energies up to 100 MeV. A smooth transition is shown between the two calculated data around 25 MeV, but the results increasingly deviate for increasing energies, where CEM95 shows a better agreement with the experimental data. The data is not sufficient to allow comparison at low energies.

The calculations of CEM95 and TNG for the ^{56}Fe (*n*,*p*) reaction cross section are shown in Fig. 9 for energies up to 100 MeV. A discontinuity in the curvature of the two calculated results is noticed above 30 MeV, but both calculations give similar results in the 5 to 30 MeV region. In this case, the low energy results from CEM95 compare better with experimental data than TNG's, which miss the low energy experimental data by about 80%.

The total cross section for *n*-induced reactions in elemental Fe is shown in Fig. 10 in the 0 to 120 MeV region. TNG shows a reasonable agreement with the experimental data from 10 to 95 MeV, but CEM95 results are much worse for all energies.

Figures 11 , 12 and 13 illustrate three typical problems that must be addressed in the future development of CETNG. The figures show the production cross sections for ^{47}Sc, ^{48}V and ^{46}Sc, respectively, from *p*-induced reactions in elemental Fe. Fig. 11 shows that TNG results are in reasonable agreement with the experimental data from activation threshold to 90 MeV, but the data oscillate strongly, because a large quantity of independent data must be gathered for the analysis. On the other

hand, CEM95 cross sections are not so good for energies below 150 MeV, but results improve for increasing energies. In this case, a better OM parametrization is expected to produce improved results in the PE region.

TNG results in Fig. 12 show reasonable qualitative agreement with the experimental data from the activation energy to 90 MeV. CEM95 results are good only for energies above 220 MeV. The region close to the activation energy is not correctly calculated by TNG, and CEM95 results are not good in the energy range below 220 MeV. It is reasonable to expect better results in the 90 to 220 MeV region from using the spin distribution of TNG in the extended region above 90 MeV, as explained in Ref. [28]. Figure 13 shows the production cross section of ^{46}Sc. Both codes give bad results in this case. TNG misses the activation threshold and the data points between 65 MeV and 100 MeV. CEM95 results are not good for energies below 190 MeV, but the estimate is good in the 200 to 300 MeV range. In this case a more accurate OM description in the 70 to 200 MeV range will possibly improve the calculation.

In summary, the calculations discussed in this report show some disagreement with the experimental data in locating peaks and activation thresholds for the analyzed reactions. There are also data regions which are not properly treated by both codes, but in most cases the results from CETNG show important improvements, particularly in the transition region between TNG and CEM95, where the PE emissions are most important. Another major problem to be addressed in future development of CETNG is the production of pions and some complex particles not yet correctly accounted for in TNG (e. g., d, t and ^{3}He).

Despite these shortcomings, the results already show the complementary functions that TNG an CEM95 have in the description of all analyzed reactions. Together with the new developments presented in Ref. [28], the above results generate optimism about the possibility of using CETNG as a consistent cross section evaluation tool for energies up to 5 GeV.
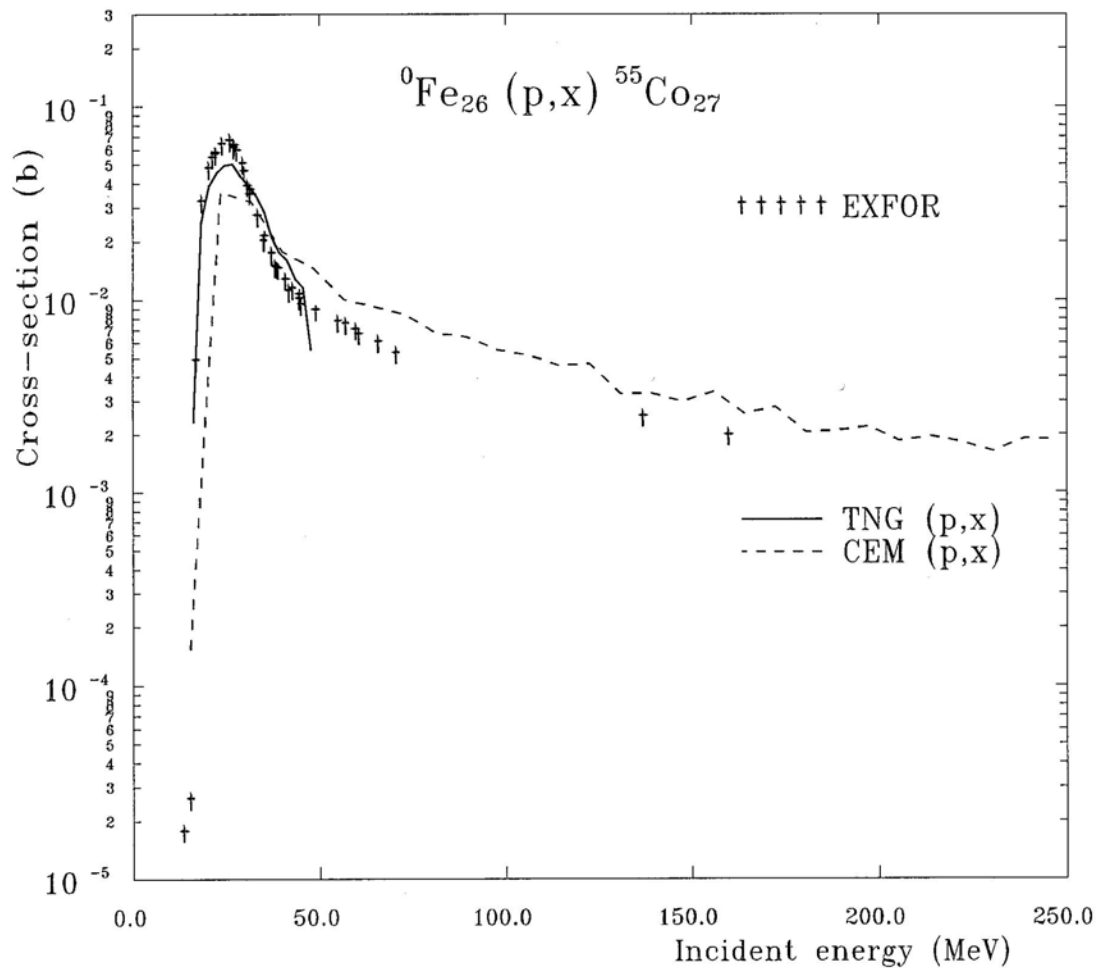
Figure 1 Production cross section for ^{55}Co with *p*-induced reactions in elemental Fe, in comparison with EXFOR data. TNG shows good agreement with the experimental data from the activation threshold to about 45 MeV and CEM95 has a reasonable agreement for E_{inc} above 30 MeV. In the 30 to 40 MeV range TNG and CEM95 calculations essentially coincide.
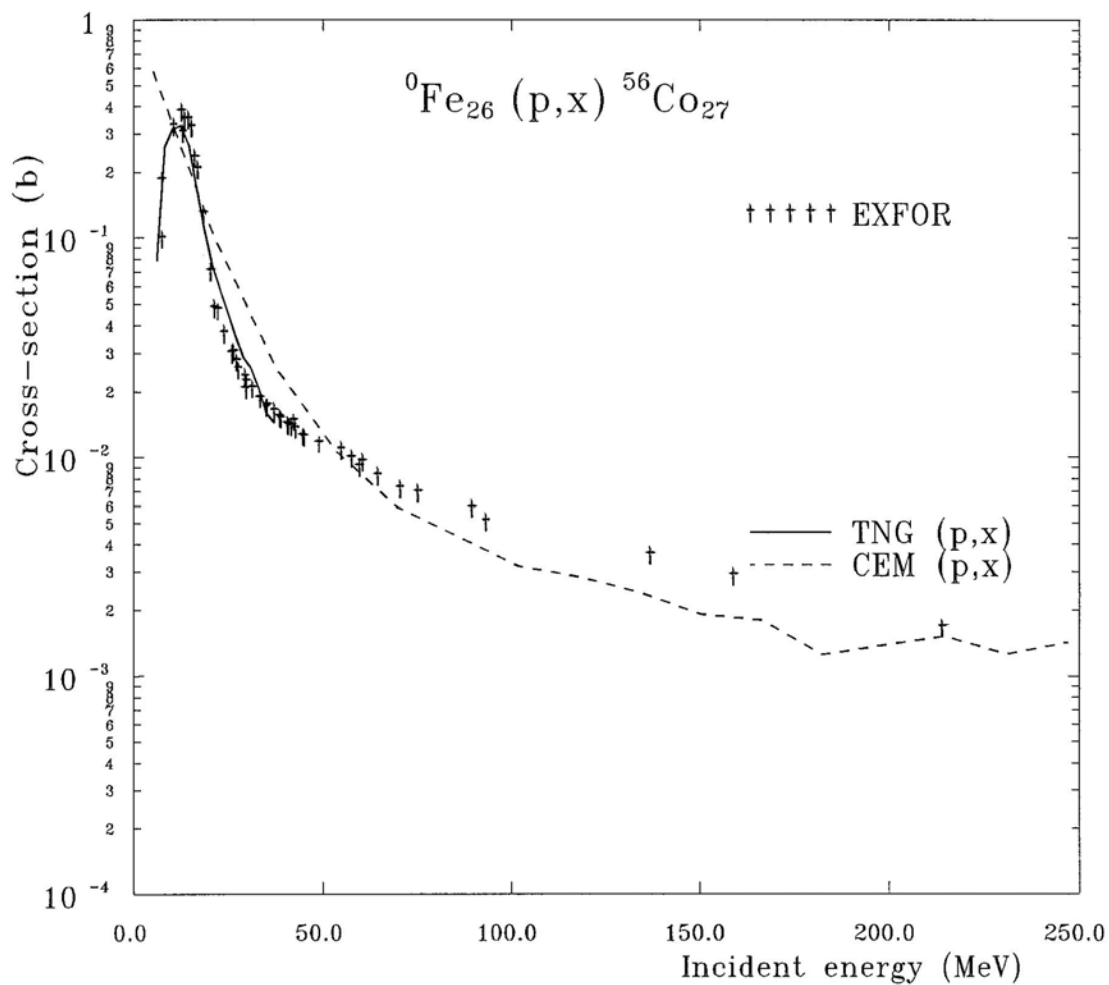
Figure 2 Production cross section for ^{56}Co with *p*-induced reactions in elemental Fe. The TNG calculation shows good agreement with the experimental data from the activation
threshold to about 45 MeV and CEM95 has reasonable agreement for E_{inc} above 50 MeV. For energies below 50MeV TNG is clearly more accurate than CEM95.
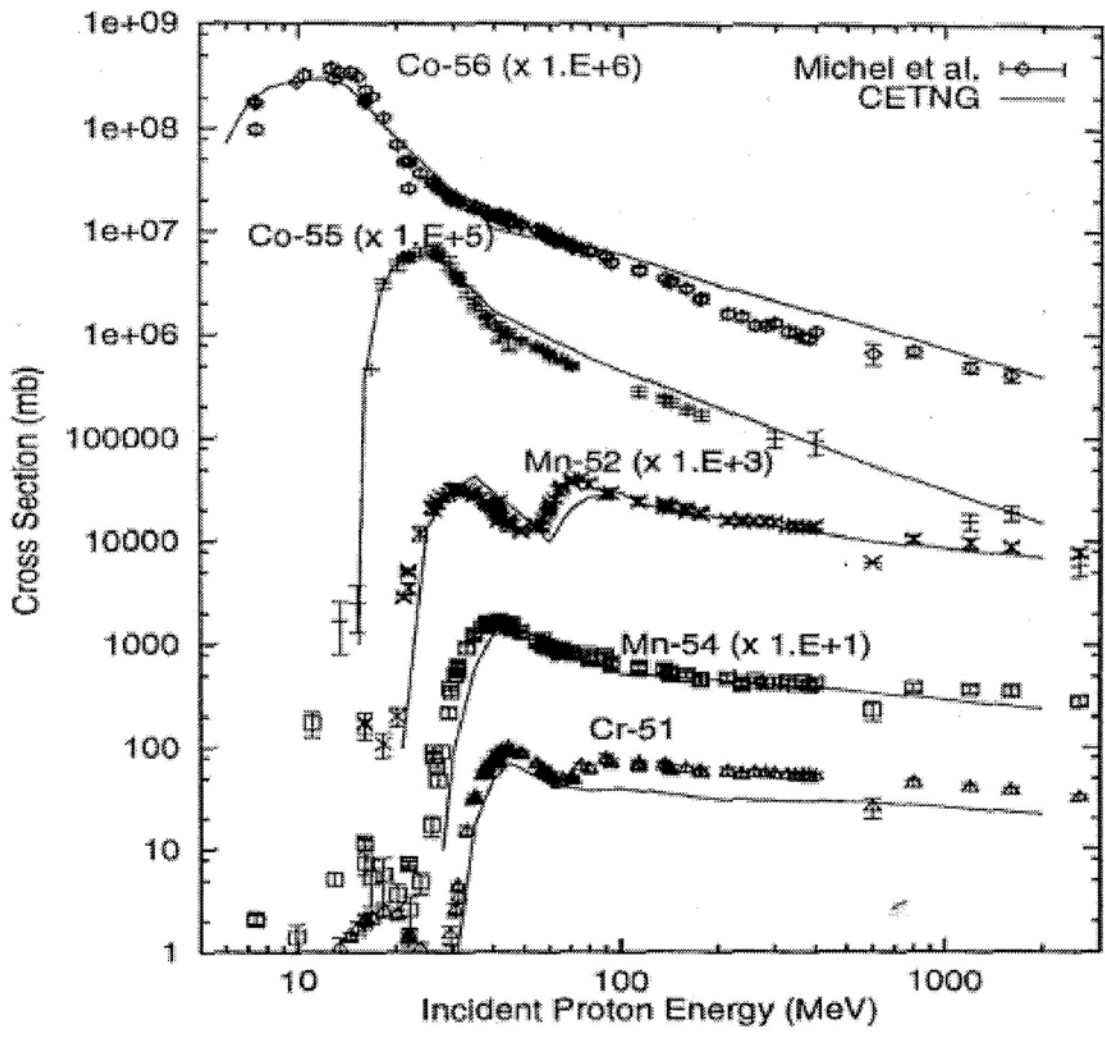
Figure 3 CETNG cross-section calculations for production reactions induced by protons in iron for various radionuclides.
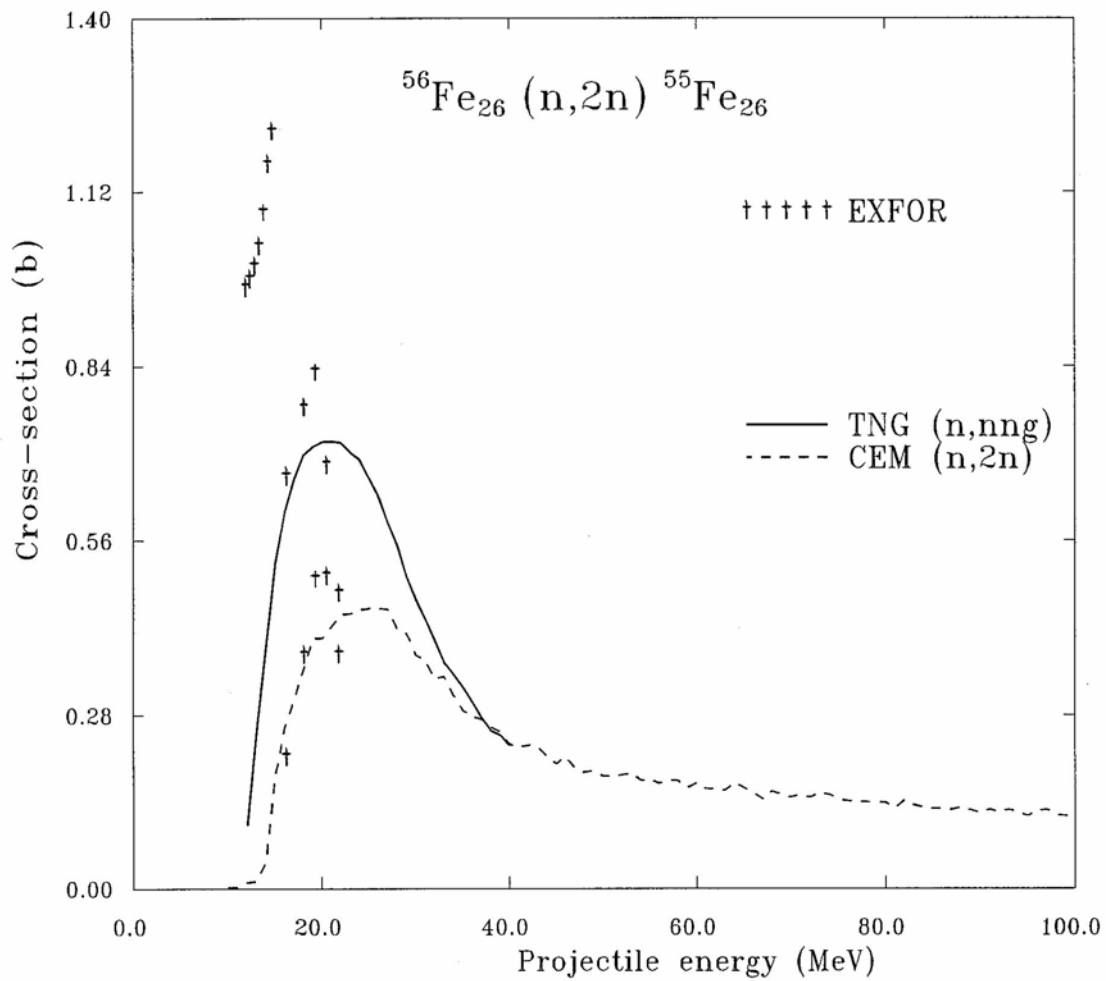
Figure 456-Fe (*n,2n*) cross sections calculated with CEM95 and TNG, for incident energies up to 100 MeV. One notices the smooth transition between the two calculations around 40 MeV.
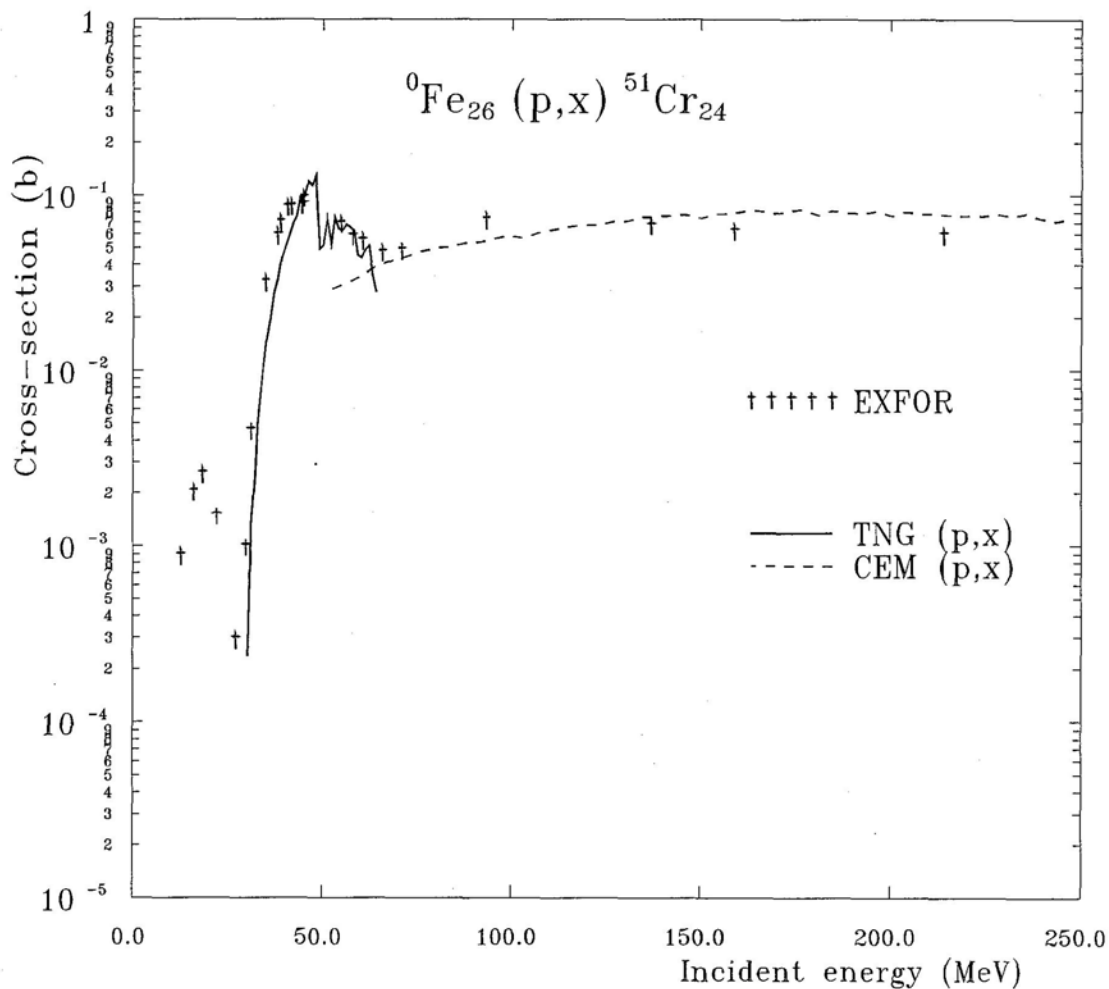
Figure 5 Production cross section for ^{51}Cr with *p*-induced reactions in elemental Fe. TNG and CEM95 calculations together give a reasonable account of the experimental results for all energies in the 30 to 250 MeV region. The peak around 20 MeV, due to the ^{54}Fe(p,p ^{3}He) reaction, cannot be described in the present version of TNG.
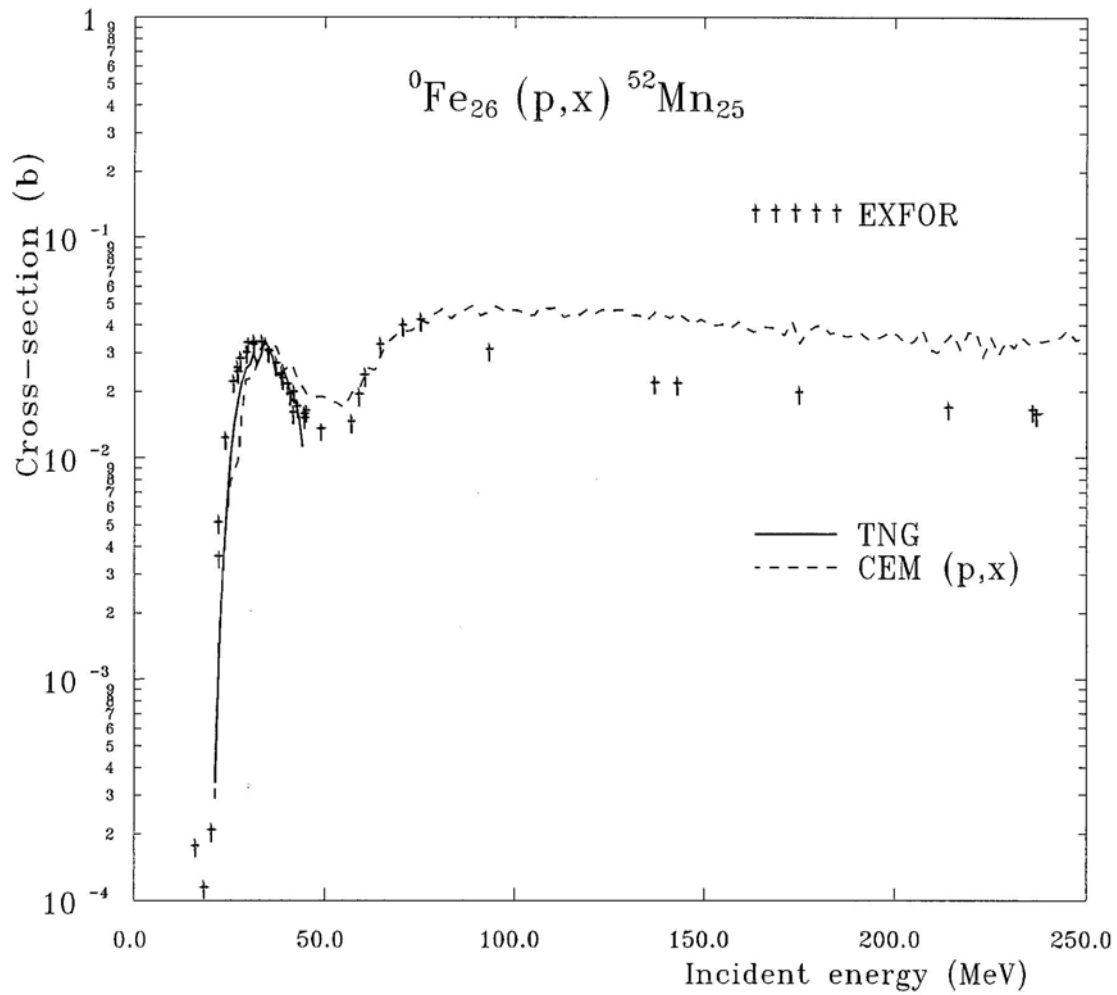
Figure 6 Production cross section for ^{52}Mn with *p*-induced reactions in elemental Fe. The TNG calculation shows good agreement with the experimental data from the activation threshold to about 45 MeV. CEM95 misses the experimental data above 80 MeV but is close to the TNG estimate in the low energy region.
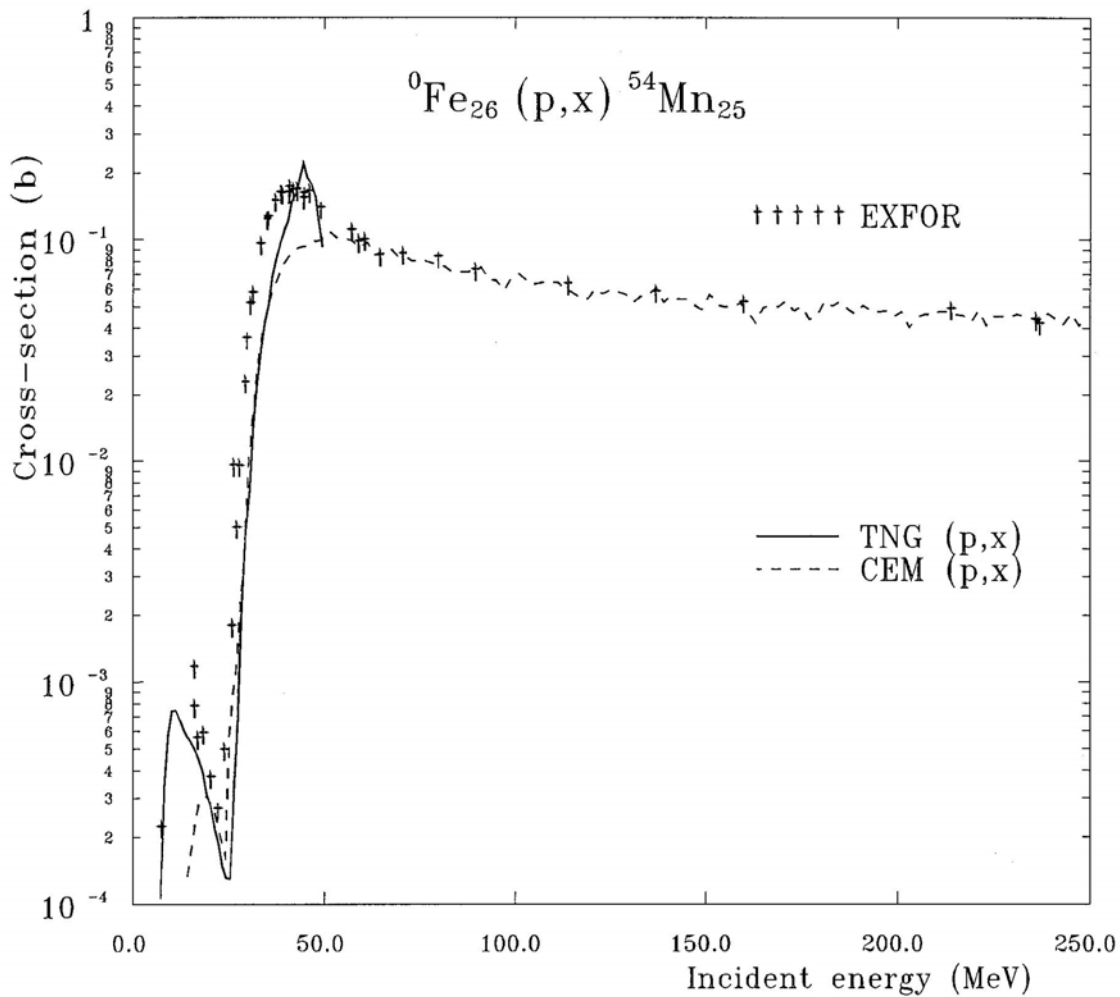
Figure 7 Production cross section for ^{54}Mn with *p*-induced reactions in elemental Fe. The TNG calculations show reasonable agreement with the experimental data from the activation thresholds to about 50 MeV and, for energies from 60 to 250 MeV, the agreement of CEM95 calculations with experimental data is excellent. The general combined result of TNG plus CEM95 is reasonable or good for all energies.
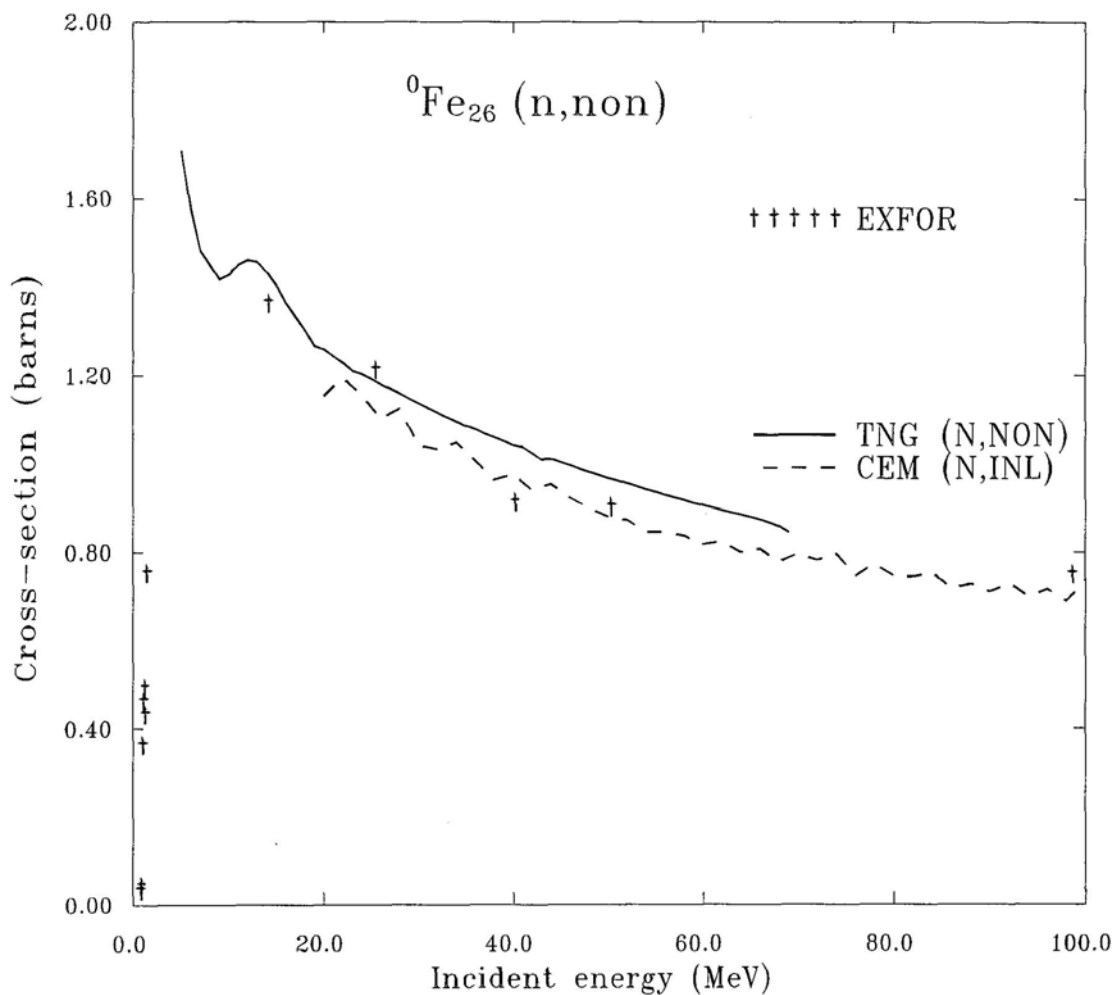
Figure 8 Nonelastic cross section in elemental Fe. The data calculated with CEM95 and TNG show a smooth transition around 25 MeV, but the results increasingly differ for increasing energies, where CEM95 shows a better agreement with the experimental data.

$^{56}Fe_{26}$ (n,p) $^{56}Mn_{25}$

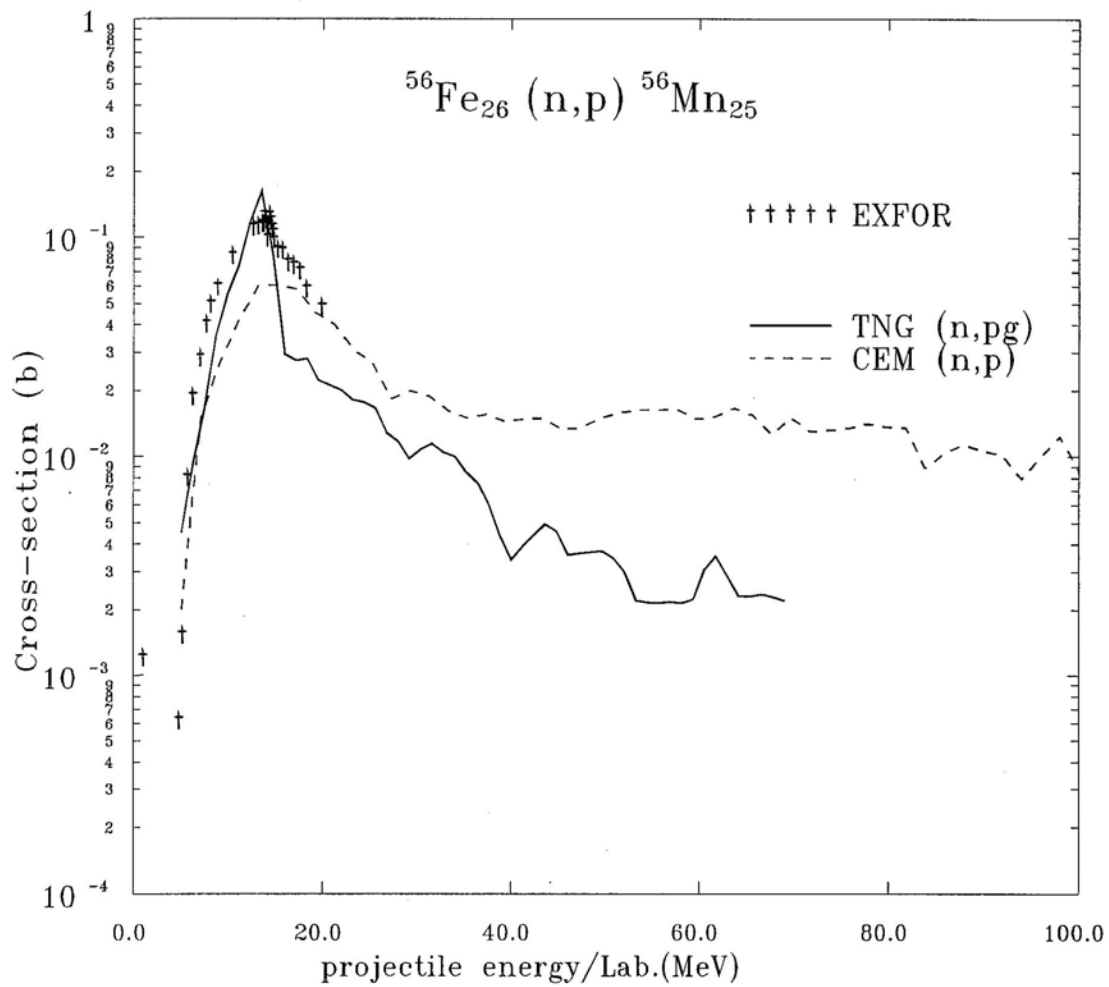† † † † † EXFOR

—— TNG (n,pg)
- - - CEM (n,p)

Figure 9 56-Fe (*n,p*) cross section. There is a discontinuity in the curvatures of the calculated data of CEM95 and TNG above 30 MeV. Both calculations give similar results in the 5 to 30 MeV region where the CEM95 results are better than the TNG results.
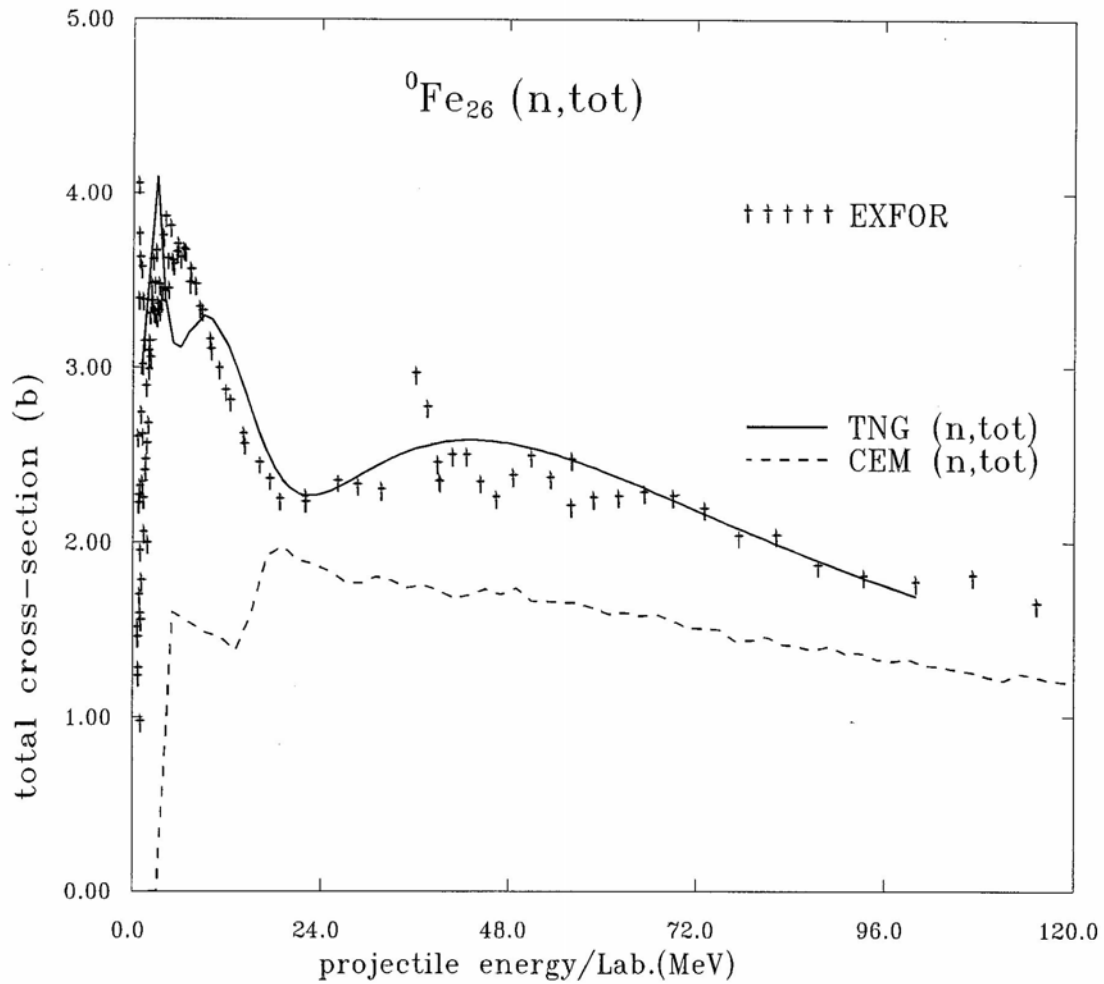
Figure 10 Total cross section for *n*-induced reactions in elemental Fe. TNG shows a reasonable agreement with the experimental data from 10 to 80 MeV. CEM95 results are much worse.
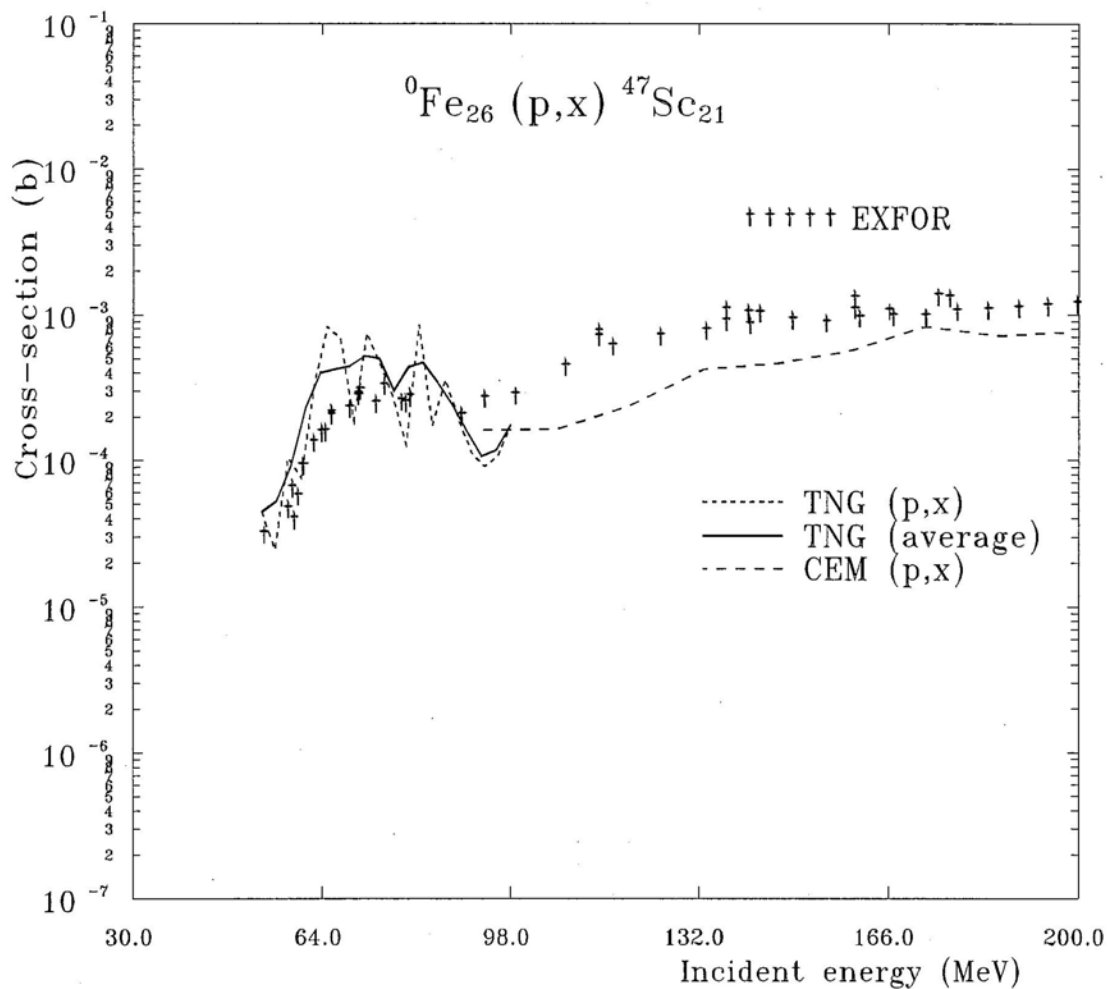
Figure 1147-Sc production reaction in elemental Fe. TNG results strongly oscillate but show a reasonable agreement, on the average, with the experimental data from activation threshold to about 90 MeV. CEM95 calculated cross sections are not good for energies below 150 MeV, but the result improves for increasing energies.
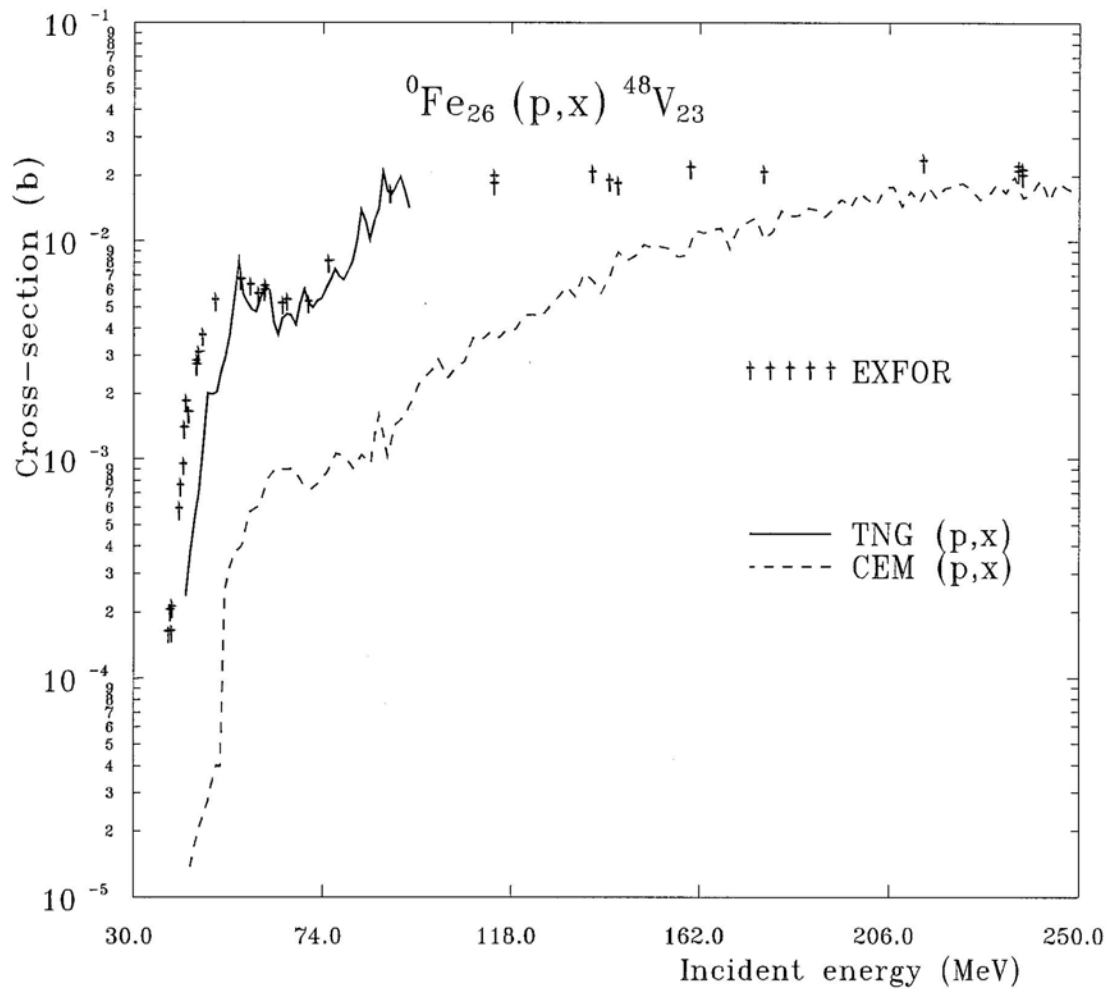
Figure 12 48-V production reaction in elemental Fe. TNG shows a reasonable qualitative agreement with the experimental data from activation threshold to 90 MeV but the region close to the activation energy is not correctly described. CEM95 results are not good in almost the whole energy interval but the estimate improves for increasing energies.

Figure 1346-Sc production cross section from *p*-induced reactions in elemental Fe. Both codes do not give good results in this case. TNG misses the activation threshold and the points between 65 MeV to 100 MeV. CEM95 results are not good for energies below 190 MeV, but the estimate is good in the 200 to 300 MeV range.

ACKNOWLEDGMENTS

REFERENCES
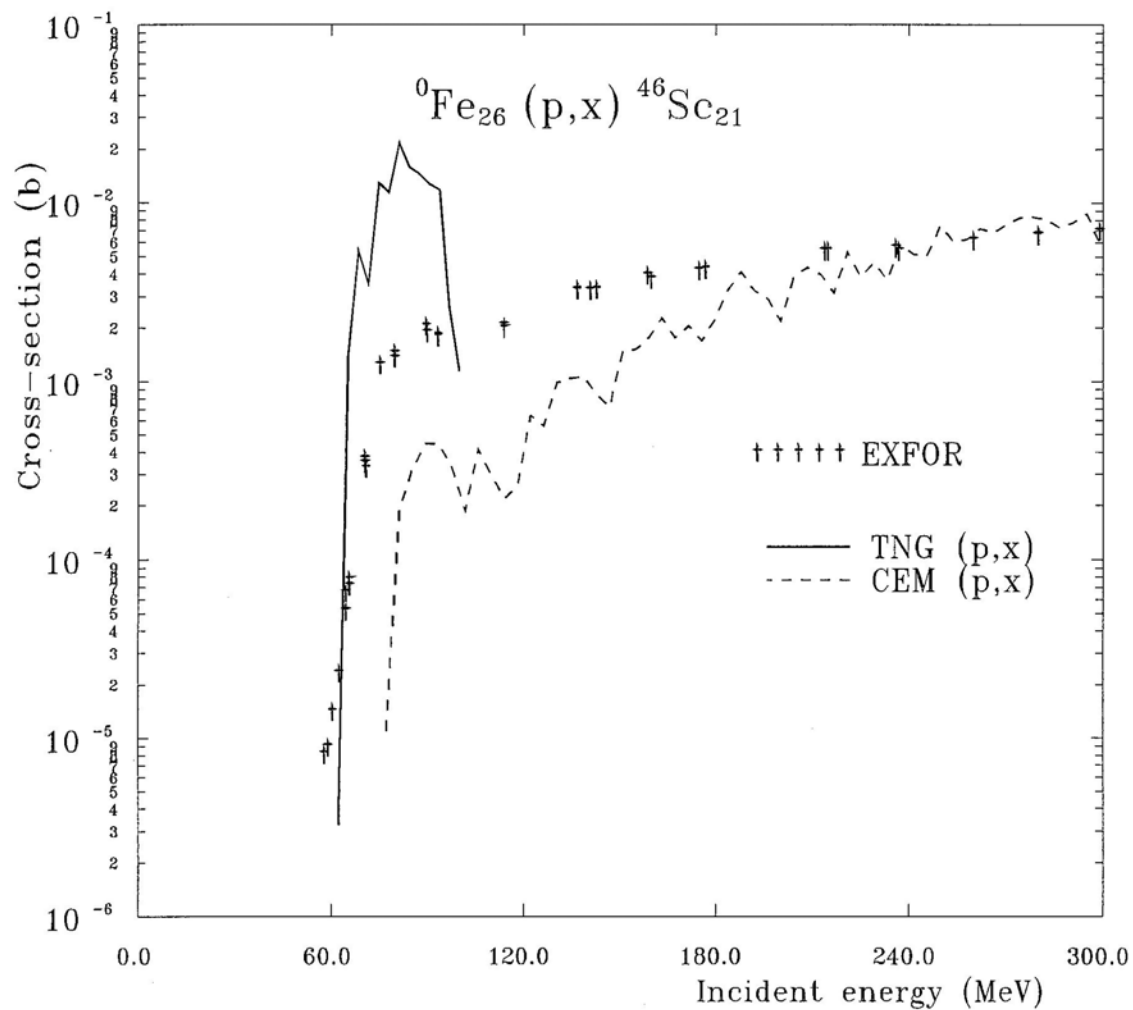
[1] M. B. Chadwick *et al., Nucl. Sci. Eng.* **131**, 293 (1999).

[2] S. G. Mashnik, *"User's Manual for the Code CEM95"*, Bogoliubov Laboratory of Theoretical Physics, Joint Institute of Nuclear Physics, Moscow, Russia (1995). K. K. Gudima, S. G Mashnik and V. D. Toneev, *Nucl. Phys. A* 401, 329 (1983).

[3] C. Y. Fu, *A Consistent Nuclear Model For Compound and Precompound Reactions with Conservation of Angular Momentum*, Report ORNL/TM-7042 (1980), Oak Ridge National Laboratory, U.S.A.; K.
Shibata and C. Y. Fu, *Recent Improvements of the TNG Statistical Model Code*, ORNL/TM-10093, (August 1986);
C. Y. Fu, *Nucl. Sci. Eng.* **86**, 344 (1984);
C. Y. Fu, *Nucl. Sci. Eng.* **92**, 440 (1986);
C. Y. Fu, *Nucl. Sci. Eng.* **100**, 61 (1988);

[4] C. Y. Fu e T. A. Gabriel, "CALOR As a Single Code Including a Modular Version of HETC" pp.23-27 in *Proc. Fourth Workshop On Simulating Accelerator Radiation Environments (SARE4)*, Knoxville, Tennessee (Sep. 14-16, 1998), Ed. T. A. Gabriel, Oak Ridge National Laboratory.

[5] H. Bertini, *Phys. Rev.* **131**, 1801 (1963)

[6] H.A. Bethe, *Phys. Rev.* **50**, 332 (1936);
H.A. Bethe, *Rev. Mod. Phys.* **9**, 69 (1937);
H.A. Bethe, *Phys. Rev.* **53**, 675 (1938).

[7] P.G. Young, E.D. Arthur and M.B. Chadwick, *Comprehensive Nuclear Model Calculations Introduction to the Theory and Use of the GNASH Code,* Technical Report LA-12343-MS (July 1992), Los Alamos National Laboratory, U.S.A.; pg. 227 in *Proceedings of the Workshop on Nuclear Reaction Data and Nuclear Reactors, Physics, Design and Safety*, Vol.1,(Eds. A. Gandini and G. Reo, World Scientific, Singapore, 1998).

[8] I. Ribansky, P. Oblozinsky, and E. Betak, *Nucl. Phys.* **A205**, 545 (1973).

[9] J.J. Griffin, *Phys. Rev. Lett.* **17**, 478 (1966);
M. Blann, *Phys. Rev. Lett.* **27**, 337 (1971).

[10] K. K. Gudima, G.A. Ososkov and V. D. Toneev, *Yad. Fiz.* **21**, 260 (1975);
K. K. Gudima and V. D. Toneev, pp 262 in *Proc. 6th. Int. Conf. on High Energy Physics and Nuclear Structure (Santa Fe, 1975),* Abstr. of Contributed Papers; pp 79 in *Proc. 5th. Int. Symp. on Interactions of Fast Neutrons with Nuclei* (Gaussig, GDR, 1977) ZfK-324.

[11] R. Serber, *Phys. Rev.* **72**, 1114 (1971)

[12] C. Kalbach-Cline and M. Blann, *Nucl. Phys. A* **172**, 1971 (225).

[13] F. C. Williams, Jr., *Nucl. Phys. A* **166**, 231 (1971).

[14] C. Kalbach-Cline, *Nucl. Phys. A* **210**, 1973 (590).

[15] V.I. Komarov *et al..*, *Nucl. Phys. A* **326**, 297 (1979);
S.G. Mashnik and S. Tesch, *Z. Phys.* **A312** (1983) 259;
S.G. Mashnik, pp 172 in *Proc. 18th Winter School Leningrad Inst. Nucl. Phys.*, vol. 3 (Leningrad, 1983);
V.N. Baturin *et al.*, Preprint *LINP-1302,* Leningrad (1987);
S.G. Mashnik, *Nucl. Phys. A* **568**, 703 (1994);
S.G. Mashnik, pp 100 in *Proc. 7th Int. Conf. on Nucl. Reaction Mechanisms,* Varenna, June 6-11, 1994;
S.G. Mashnik, *Revue Roum. Phys.* **37**, 179 (1992);
Proc. 20th Winter School Leningrad Inst. Nucl. Phys., vol. 3, 236 (Leningrad,1985);
Acta Phys. Pol. B24, 1685 (1993).

[16] W. Hauser and H. Feshbach, *Phys. Rev.* **87**, 366 (1952)

[17] J.E. Lynn, *Nuclear Fission and Neutron-Induced Fission Cross-Sections*, p.204, Ed. A.Michaudon, Pergamon Press (1981);
X. Bjornholm and J.E. Lynn, *Rev. Mod. Phys.* **52**, 1980 (725).

[18] F. B. Guimarães and C. Y. Fu, *TNG-GENOA User's Manual*, Technical Report ORNL/TM-2000/252 (2000), Oak Ridge National Laboratory, U.S.A.

[19] C. Kalbach-Cline, *Nucl. Phys. A* **195**, 1972 (353).

[20] C. Wasshuber PhD. *Thesis About Single-Electron Devices and Circuits*, Tech. Univ. of Vienna, Inst. of Microelectronics, Vienna, January 1997 (e-address http://www.iue.tuwien.ac.at/publications/PhD%20Theses/wasshuber).

[21] T. Ericson, *Adv. in Phys.* **9**, 423 (1960).

[22] C. Kalbach, *Z. Physik* **A283**, 401 (1977).

[23] A. Gilbert and A. G. W. Cameron, *Can. J. Phys.* **43**, 1446 (1965).

[24] J. R. Huizenga and L. G. Moretto, *Annu. Rev. Nucl. Sci.* **22**, 427 (1972);
A. V. Ignatyuk and Yu. N. Shubin, *Sov. J. Nucl. Phys.* **8**, 660 (1969);
V. Ignatyuk, Yu. Sokolov and Yu. N. Shubin, *Sov. J. Nucl. Phys.* **18**, 510 (1974);
A. V. Ignatyuk, J. L. Weil, S. Raman and S. Kahane, *Phys. Rev. C* **47**, 1504 (1993);
A.V. Ignatyuk and Yu. Sokolov, *Sov. J. Nucl. Phys.* **17**, 376 (1973).

[25] L.G. Moretto, *Nucl. Phys.* **A243**, 77 (1975).

[26] J.Bardeen, L.N.Cooper e J.R.Schrieer, *Phys. Rev.* **106**, 162 (1957);
J.Bardeen, L.N.Cooper e J.R.Schrieer, *Phys. Rev.* **108**, 1175 (1957).

[27] L. McFadden and G. R. Satchler, *Nucl. Phys.*, **84**, 177 (1966).

[28] C. Y. Fu, F. B. Guimarães and L. C. Leal, "Combining Semi-Classical and Quantum Mechanical Methodologies for Nuclear Cross-Section Calculations Between 1 Mev and 5 GeV," *Proc. International Conference on Nuclear Data for Science and Technology*, Oct. 7-12, 2001, Tsukuba, Tsukuba, Ibaraki, Japan.

[29] EXFOR - Experimental Nuclear Reaction Data File - web site at the Brookhaven National Laboratory (http://www.nndc.bnl.gov/nndc/exfor/).

[30] RIPL - Reference Input Parameter Library for theoretical calculations of nuclear reactions - web site at the Nuclear Data Centre of the International Atomic Energy Agency (http://www-nds.iaea.or.at/ripl/).

[31] A. G. W. Cameron, *Can. J. Phys.* **35**, 1021 (1957). and *Z. Phys.* **A35**, 1021 (1957).

[32] A. V. Malyshev, *Level Densities and Structure of Atomic Nuclei*, Ed. Atomizdat, Moscow (1969).

[33] A. Mengoni and Y. Nakajima, *J. Nucl. Sci. Tech.*, **31** no.2, 151 (1994); JAERI-M 93-177, Japan Atomic Energy Research Institute, Sep. 1993.

[34] W. D. Myers and W. S. Swiatecki, *Ark. Fys.*, **36**, 343 (1967).

[35] H. Feshbach, A. Kerman and S. Koonin, *Ann. Phys.* (N.Y.) **125**, 429 (1980).

[36] D. M. Wharton and D. K. Olsen, *LSFODFA Generalized Nonlinear Least-Squares Fitting Program For Use With ORELA odf Files*, ORNL/TM-6545/R4 Oak Ridge National Laboratory Technical Report, Oak Ridge, Tenn., USA (December 1978).

[37] R. Michel *et al.*, *Nucl. Inst. Meth. Phys. B* **129**, 153 (1997).

[38] A. J. Koning, J. P. Delaroche, 0. Bersillon, *Nucl. Inst. Meth. Phys. A* **414**, 49 (1998).

INTERNAL DISTRIBUTION

1.	Central Research Library	21.	Joseph N. Herndon
2.	Laboratory Records-RC	22.	David M. Hetrick
2-3.	Laboratory Records-OSTI	23.	Daniel F. Hollenbach
4.	Daniel W. Bardayan	24.	Calvin M. Hopper
5.	James R. Beene	25.	Hamilton T. Hunter
6.	Fred E. Bertrand Jr.	26.	Daniel T. Ingersoll
7.	Jeff C. Blackmon	27.	Jeffrey O. Johnson
8.	Bryan L. Broadhead	28.	Bernadette Lugue Kirk
9.	Herve Derrien	29.	Nancy M. Larson
10.	Felix C. Difilippo	30.	Luiz C. Leal
11.	Michael E. Dunn	31.	Richard A. Lillie
12.	Chia Y. Fu	32.	Cecil V. Parks
13.	T. A. Gabriel	33.	Lester M. Petrie Jr.
14.	Ian C. Gauld	34.	S. Ram Raman
15.	Jess C. Gehin	35.	Bradley T. Rearden
16.	Sedat Goluoglu	36.	John-Paul Renier
17.	Jorge Gomez Del Campo	37.	Robert T. Santoro
18.	Franz Galmaier	38.	Royce O. Sayer
19.	Norman Maurice Greene	39.	John C. Wagner
20.	Klaus H. Guber	40.	RSICC

EXTERNAL DISTRIBUTION

41. C. Bastien, Central Bureau for Nuclear Measurements, Steenweg op Retie, 2240 Geel, Belgium
42. David Beck, U.S. Department of Energy, 1000 Independence Ave. SW, 4A-019 Washington, DC 20585
43. H. Beer, Forschungszentrum Karlsruhe, IK, BAV 425, Postfach 3640, D-76021, Karlsruhe, Germany
44. Timothy E. Beville, U.S. Department of Energy, 19901 Germantown Rd., Germantown, MD 20874
45. Thomas M. Black, U.S. Department of Energy, 19901 Germantown Road MS A-359, Germantown, MD 20874-1290
46. P. Blaise, DER/SPRC/LEPH, Batiment 230, Centre d'Etudes de CADARACHE, 13108 Saint Paul-lez-Durance, France
47. R. Block, Rensselaer Polytechnic Institute, Troy, NY 12180-3590
48. William M. Blumberg, U.S. Nuclear Regulatory Commission, One Flint North, Mail Stop 10 H4, 11555 Rockville Pike, Rockville, MD 20852-2738
49. O. Bouland, DER/SPRC/LEPH, Batiment 230, Centre d'Etudes de CADARACHE, 13108 Saint Paul-lez-Durance, France

50. J. Burke, Gaerttner LINAC Laboratory, Rensselaer Polytechnic Institute, Department of Environmental and Energy Engineering, Troy, NY 12180-3590

51. D. Cabrilla, U.S. Department of Energy, NE-40, 19901 Germantown Road, Germantown, MD 20874-1290

52. D. E. Carlson, U.S. Nuclear Regulatory Commission, Reactor and Plant System Branch, Division of System Research, Office of Nuclear Regulatory Research, MS T-10 G6, RM T-10, 17, Washington, DC 20555-0001

53. R. F. Carlton, Middle Tennessee State University, Department of Chemistry and Physics, Murfreesboro, TN 37132

54. E. Caro, Lockheed Martin Corporation, P.O. Box 1072, Schenectady, NY 12301-1072

55. M. B. Chadwick, Los Alamos National Laboratory, MS B243 T-16, Los Alamos, NM 87545

56. Jonghwa Chang, Korea Atomic Energy Research Inst., Nuclear Data Evaluation Lab., P. O. Box 105, Yusung, Taejon 305-600, Korea

57. David H. Crandall, U.S. Department of Energy, DP-18/4A-045, Dir., Inertial Fusion/Natl. Ignition Facility Project, 1000 Independence Ave. SW, Washington, DC 20585

58. D. E. Cullen, Lawrence Livermore National Laboratory, MS L-298, P. O. Box 808, Livermore, CA 94550

59. P. Finck, Argonne National Laboratory, Reactor Analysis Division, Bldg 208, Argonne, IL 60439

60. S. C. Frankle, X-TM, MS B226, Los Alamos National Laboratory, Los Alamos, NM 87545

61. W. Furman, Joint Inst. of Nuclear Research, P.O. Box 79, 141980 Dubna, Russian Federation

62. Srinivasan Ganesan, Head, Nuclear Data Section, Indira Gandhi Centre for Atomic Research, Kalpakkam 603 102, Tamilnadu, India

63. Frank Gunsing, Centre D'Etudes De Saclay, DSM/DAPNIA/SPhN, F-91191 Gif-sur-Yvette Cedex, France

64. G. M. Hale, Los Alamos National Laboratory, T-2, MS B243, Los Alamos, NM 87545

65. Akira Hasegawa, Nuclear Data Center, Japan Atomic Energy Research Institute, Tokai-mura, Naka-gun, lbaraki-ken 319-11, Japan

66. R. N. Hwang, Argonne National Laboratory, Reactor Analysis Division, Bldg 208, Argonne, IL 60439

67. R. P. Jacqmin, DER/SPRC/LEPH, Batiment 230, Centre d'Etudes de CADARACHE, 13408, Saint Paul-lez-Durance, France

68. N. Janeva, Bulgarian Academy of Sciences, 72, Boul, Tzarigradsko shosse, Sofia 1784, Bulgaria

69. F. Kappeler, Forschungszentrum Karlsruhe, IK, BAV 425, Postfach 3640, D-76021, Karlsruhe, Germany

70. G. Leinweber, Gaerttner LINAC Laboratory, Rensselaer Polytechnic Institute, Dept. of Environmental and Energy Engineering, Troy, NY 12180-3590

71. R. Little, Los Alamos National Laboratory, X-TM, MS B226, Los Alamos, NM 87545

72. C. Lubitz, Knolls Atomic Power Laboratory, P. O. Box 1072, Schenectady, NY 12301

73. C. Mounier, CEN Saclay, DMT/SERMA/LENR, , 91191 Gif Sur Yvette Cedex, France

74. C. Nordborg, OECDNEA, Le Seine St-Germain 12, Boulevard Iles, 92130, Issy-les-Moulineaux, France

75. A. Nouri, OECD/NEA Data Bank, Le Seine Saint Germain 12 Bd des Iles, 92130 Issy-les-Moulineaux, France

76. S. Y. OH, Nuclear Data Evaluation Lab., Korea Atomic Energy Research Institute, P. O. Box 105, Yusung Taejon, 305-600 Korea

77. A. Popov, Frank Laboratory of Neutron Physics, Joint Institute for Nuclear Research, RU-141980 Dubna, Moscow Region, Russia
78. C. Raepsaet, CEN Saclay, DMT/SERMA/LEPP, 91191, Gif Sur Yvette Cedex, France
79. M. Salvatores, DRN/P, Batiment 707, C. E. CADARACHE, 13108, Saint Paul-lez-Durance, France
80. E. Sartori, OECDNEA, Le Seine St-Germain 12, Boulevard Iles, 92130, Issy-les-Moulineaux, France
81. O. A. Shcherbakov, Petersburg Nuclear Physics Institute, 188350 Gatchina, Leningrad District, Russia
82. R. Shelley, Central Bureau for Nuclear Measurements, Steenweg op Retie, 2240 Geel, Belgium
83. K. Shibata, Japan Atomic Energy Research Institute, Nuclear Data Center, Tokai-mura Naka-gun, Ibaraki-ken 319-11, Japan
84. P. Siegler, Central Bureau for Nuclear Measurements, Steenweg op Retie, 2240 Geel, Belgium
85. Mihaela Sin, Bucharest University Nuclear Physics Department, P.O. Box MG-11, RO-76900 Bucharest-Magurele, Romania
86. A. B. Smith, Argonne National Laboratory, TD 362 D216, Argonne, IL 60544
87. D. L. Smith, Argonne National Laboratory, TD-360-L106, Argonne, IL 60544
88. J. P. Weinman, Lockheed Martin Corporation, P.O. Box 1072, Schenectady, NY 12301-1072
89. Phillip G. Young, Los Alamos National Laboratory, MS B243 T-16, Los Alamos, NM 87545